NKS-453
ISBN 978-87-7893-546-5

Analysis of the Performance of $LaBr_3$ Detectors for Fresh Fallout Response (PERLAD)

M.Dowdall[1]
Kari Peräjärvi[2]
Tero Karhunen[2]
Sara Ehrs[3]
Charlotte Alfast Espensen[4]
Gísli Jónsson[5]

[1] Norwegian Radiation and Nuclear Safety Authority
[2] Radiation and Nuclear Safety Authority (STUK), Finland
[3] Swedish Radiation Safety Authority
[4] Danish Emergency Management Agency (DEMA)
[5] Icelandic Radiation Safety Authority

January 2022

Abstract

With spectral resolution of approximately 3 % at 662 keV, $LaBr_3$ scintillators exhibit substantial improvements over sodium iodide scintillators with a resolution of 6-7 % for crystals of comparable sizes and fast emission relative to NaI and HPGe. $LaBr_3$ crystals are available in sizes up to 3×3 inches and this availability has led to an increase in the prevalence of such detectors for a variety of purposes. These include as hand held detectors for in-field use, in conventional laboratory situations and for direct monitoring of radioactive contaminants. Direct measurement of airborne contamination is made complicated for any detector type due to the necessity to generate efficiency data for a geometry which is in effect impossible to replicate. While estimates of efficiency may be obtained using deterministic calculations, the need to account for elements of the detector assembly aside from the detector complicates the process. This project investigates the use of such detectors for the direct measurement of airborne and ground deposited contamination using Monte Carlo simulation for the assessment of efficiency in field use configurations.

Key words

$LaBr_3$, efficiency, Monte Carlo, emergency preparedness

NKS-453
ISBN 978-87-7893-546-5
Electronic report, January 2022
NKS Secretariat
P.O. Box 49
DK - 4000 Roskilde, Denmark
Phone   +45 4677 4041
www.nks.org
e-mail   nks@nks.org

Analysis of the Performance of $LaBr_3$ Detectors for Fresh Fallout Response (PERLAD)

Final Report from the NKS-B PERLAD project (Contract: AFT/B(21)7)

M.Dowdall[1]

Kari Peräjärvi [2]

Tero Karhunen [2]

Sara Ehrs [3]

Charlotte Alfast Espensen [4]

Gísli Jónsson [5]

[1] Norwegian Radiation and Nuclear Safety Authority

[2] Radiation and Nuclear Safety Authority (STUK), Finland

[3] Swedish Radiation Safety Authority

[4] Danish Emergency Management Agency (DEMA)

[5] Icelandic Radiation Safety Authority

Table of contents

Acknowledgements

NKS conveys its gratitude to all organizations and persons who by means of financial support or contributions in kind have made the work presented in this report possible.

Disclaimer

The views expressed in this document remain the responsibility of the author(s) and do not necessarily reflect those of NKS. In particular, neither NKS nor any other organisation or body supporting NKS activities can be held responsible for the material presented in this report. Mentioning of software, materials or products does not constitute an endorsement by the authors or the NKS. Materials provided as part of the project detailed in this report are intended for the use described and should not be used for purposes other than those described by the authors.

1. Introduction

With spectral resolution of approximately 3 % at 662 keV, cerium doped lanthanum bromide ($LaBr_3$: Ce, hereafter $LaBr_3$) scintillators (van Loef et al. 2001) exhibit substantial improvements over sodium iodide (NaI [Tl]) scintillators with a resolution of 6-7 % for crystals of comparable sizes and fast emission relative to NaI and HPGe. $LaBr_3$ crystals are available commercially in sizes up to 3×3 inches and this availability has led to an increase in the prevalence of such detectors in the instrument parks of a number of countries for a variety of purposes. Typically employed as hand-held radio-isotope identification devices (RIIDs), the resolution of $LaBr_3$ and other advantages in relation to portability, size, efficiency and operating costs have led to its adoption for use in other roles that were typically the domain of NaI and HPGe detector systems. These roles include monitoring and emergency response. With respect to emergency preparedness, one of the most challenging situations for any detector type is fresh fallout after a nuclear accident. In this context, a large number of isotopes may be present, many of which may have complex gamma spectra, at very different levels of activity. This presents a significant challenge for detectors as a very complex spectrum is problematic both for detectors of low resolution (such as NaI) and even for higher resolution detectors such as high purity Germanium (HPGe). Fresh fallout monitoring may also involve measurements in contexts and geometries that are difficult with respect to determination of the detector response. These include direct monitoring of airborne activity and direct monitoring of deposited contamination on the ground surface. Given that $LaBr_3$ detectors have only recently been widely adopted in the emergency response role, there has been a lack of opportunities for appraising their performance in situations involving fresh fallout. Both NaI and HPGe are relatively known quantities with respect to both laboratory and in-situ measurements of fresh fallout given they have been in widespread use during both the Fukushima and Chernobyl accidents. $LaBr_3$ was not deployed to any great extent during the former and did not exist as a commercial detector during the latter accident.

Despite the advantages conferred by a detector with good resolution, efficiency and portability, $LaBr_3$ as a detection system exhibits some inherent and potentially significant disadvantages. Primary among these is the presence of internal radioactivity within the crystal itself and some resolution weakness at energies below approximately 100 keV. Naturally occurring radioactivity due to ^{138}La and ^{227}Ac constitute the most significant drawbacks in $LaBr_3$ as a detector material.

La-138 comprises 0.09 % of naturally occurring lanthanum and has a 1.06 x 10^{11} yr. half-life and has two γ-rays: a 788.7 keV γ-ray from β-decay (34 %) to stable ^{138}Ce and a 1435.8-keV gamma ray from EC (66 %) to stable ^{138}Ba. Strong Ba *K* x-rays are also observed between 31 and 38 keV although these are of less significance for emergency preparedness purposes. Notice that the X-rays are emitted in coincidence with the 1435.8 keV gamma-rays producing sum peaks into the spectra. The 788.7 keV gamma-rays do not appear as a gaussian shape peak in the spectra since they are emitted in coincidence with the beta-particles. Ac-227 has a 21.77 yr. half-life and arises naturally within the ^{235}U series. As a chemical analogue of lanthanum, this contaminant may be found in lanthanum-based scintillators. Ac-227 decay to stable ^{207}Pb includes five α decays. While initial iterations of commercially available lanthanum halide crystals had contamination levels of 1.3 x 10^{-13} ^{227}Ac atoms/La atom this level has since been reduced by over two orders of magnitude in recent years but may potentially still affect background spectra. Irrespective of this, ^{138}La remains the primary contaminant of concern in use of $LaBr_3$ detectors for typical emergency response functions.

The PERLAD project was focused on the application of $LaBr_3$ detectors to emergency response and direct monitoring in conditions of fresh fallout from a nuclear accident. The project focused on the advantages and disadvantages of such detectors relative to standard detector types for fresh fallout monitoring, the application of various means of calibration and the applicability of current software analysis routines to $LaBr_3$ in this particular context and recommendations as to any modifications or adaptions of such routines to improve performance.

Previous attempts have been made to assess efficiencies of $LaBr_3$ detectors in the configurations employed in the PERLAD project. Urban and Vágner (2019) conducted simulations of a 1.5” by 1.5” $LaBr_3$ detector at 1 meter height (face down) for direct measurements of contaminated air volumes to assess efficiencies. Simulations were conducted for air volumes similar to those employed here. It is worth noting that the detector employed was x-rayed in order to produce the model and no attempt was made at assessing the simulations validity with respect to actual measurements. The dependance of efficiency of $LaBr_3$ detectors on the angular orientation of the detectors with respect to the incident photons has previously been appraised using simulations and actual measurements by Jedonorg et al. (2015) and Modzelewski et al. (2021).

2. Detectors

The detectors as utilized throughout the PERLAD project are as described in the following and have been denoted as Detectors 1, 2, 3, 4 and 5 for simplicity.

2.1 Detector 1.

Material: $LaBr_3$

Crystal dimensions: 38.1mm x 38.1mm.

Housing: 140 mm diameter, 315 mm length aluminum protective tube of 0,5 mm thickness housing a detector unit consisting of a PMT tube and the crystal and an MCA base unit. The space between the detector unit and the aluminum protective unit is filled with a polyurethane filler. The crystal and PMT are housed within their own aluminum tube of 0.5 mm wall thickness.

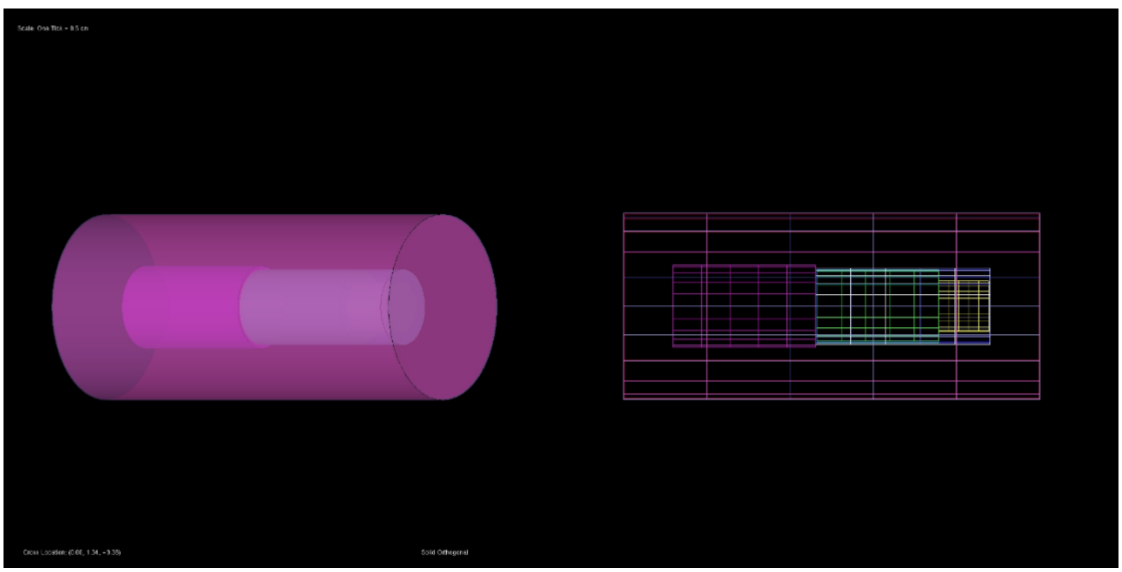

Figure 1. GEANT4 model of the $LaBr_3$ Detector 1 and housing.

Orientation and position: 2 m above ground (to crystal center), facing up.

Energy: Energy (keV) as a function of channel is described by:

$$E(c) = 3.6573 + 1.4328c + (2.3019\text{E} - 05)c^2\text{, 2048 channels}$$

Resolution: The resolution (keV) varies with energy according to the function:

$$R(E) = \sqrt{95.416 + 0.38198E}$$

2.2 Detector 2.

Material: $LaBr_3$

Crystal dimensions: 38.1mm x 38.1mm.

Housing: 58 mm diameter, 233 mm length plastic tube of 0.2 mm thickness with integral PMT tube and foam rubber filler.

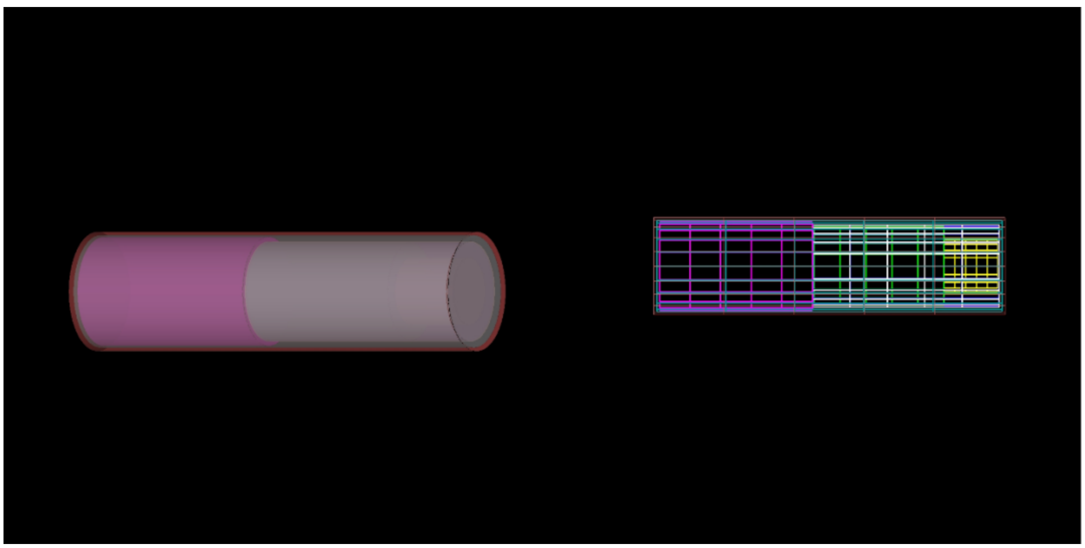

Figure 2. GEANT4 model of the $LaBr_3$ Detector 2 and housing.

Orientation and position: 1 m above ground (to crystal center), facing down

Energy: Energy (keV) as a function of channel is described by:

$$E(c) = 3.6573 + 1.4328c + (2.3019\mathrm{E}-05)c^2 \text{ , 2048 channels}$$

Resolution: The resolution (keV) varies with energy according to the function:

$$R(E) = \sqrt{95.416 + 0.38198E}$$

2.3 Detector 3.

Material: HPGe

Crystal dimensions: 50 mm diameter x 33 mm length

Housing: Integrated pump based cryo-cooler and a lithium-ion battery.

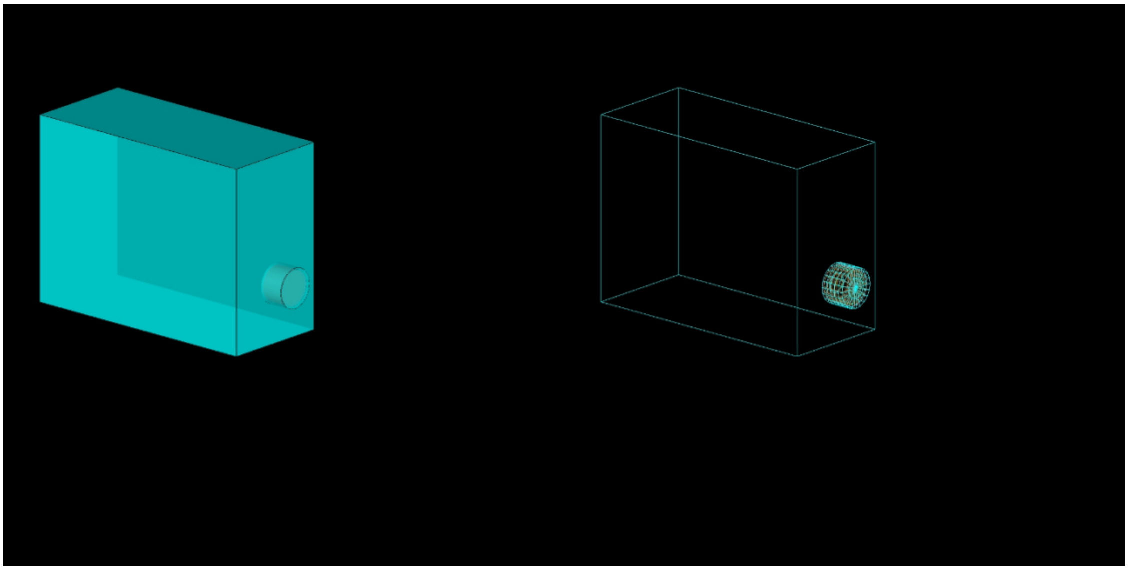

Figure 3. GEANT4 model of the HPGe Detector 3 and cooling unit.

Orientation and position: 1m above ground, facing down

Energy: Energy (keV) as a function of channel is described by:

$$E(c) = 0.28256 + 0.36587c + (3.084\mathrm{E} - 08)c^2 \text{ , 8192 channels}$$

Resolution: The resolution (keV) varies with energy according to the function:

$$R(E) = \sqrt{2.4896 + 0.00055740E}$$

2.4 Detector 4.

Material: CdZnTe

Crystal dimensions: 10 mm x 10 mm x 10 mm

Housing: 25 mm x 25 mm x 63 mm package, assumed to be 0.5 mm aluminium

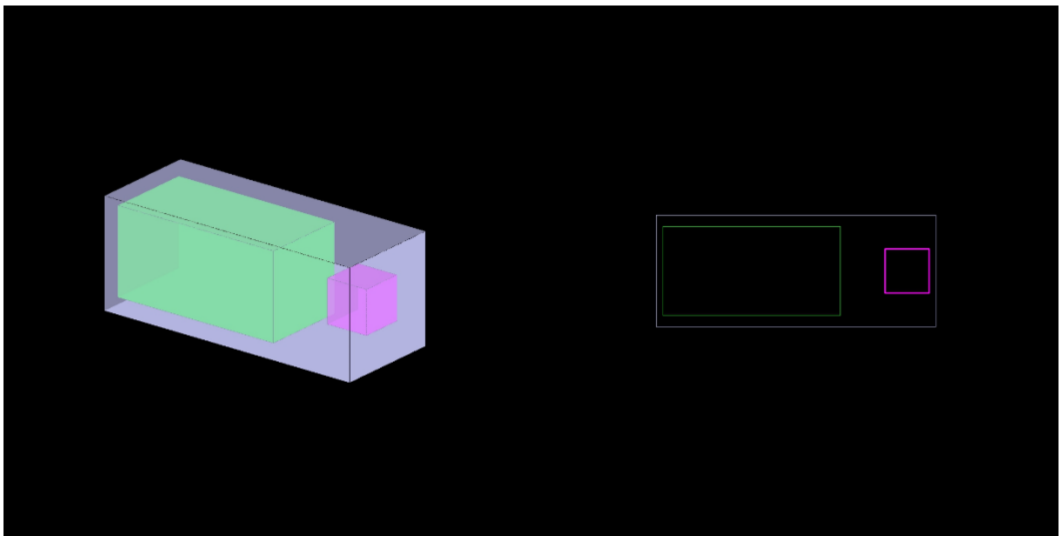

Figure 4. GEANT4 model of the CdZnTe Detector 4 and housing.

Orientation and position: 1m above ground, facing down

Energy: Energy (keV) as a function of channel is described by:

$$E(c) = 0.038559 + 0.74874c + (2.7819\text{E} - 06)c^2$$, 4096 channels

Resolution: The resolution (keV) varies with energy according to the function:

$$R(E) = \sqrt{57.792 + 0.1898E}$$

2.5 Detector 5.

Material: NaI

Crystal dimensions: 38.1 mm diameter x 25.4 mm length

Housing: Integrated PMT and detector housing, MCA base. No protective housing in addition to the unit housing.

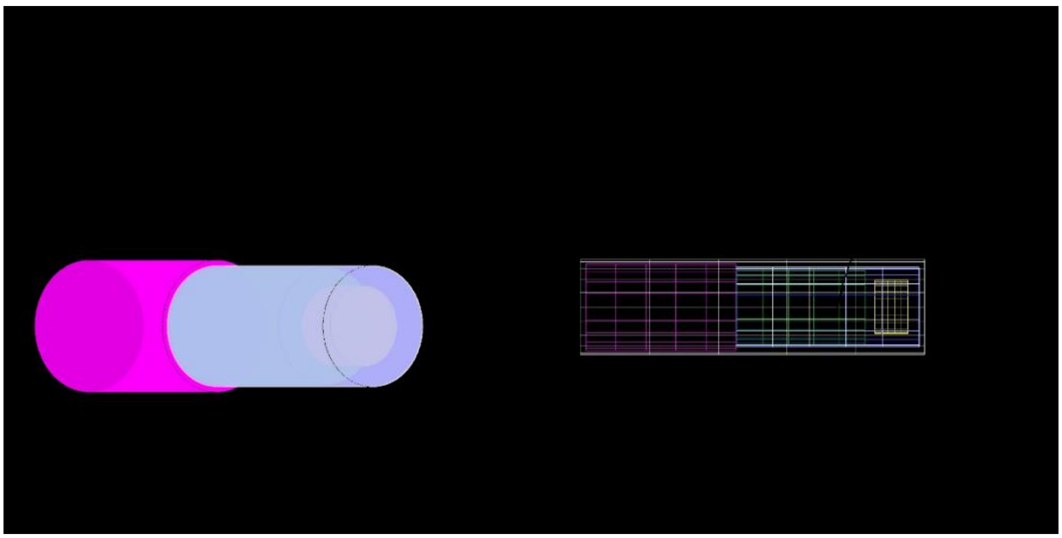

Figure 5. GEANT4 model of the NaI Detector 5 and housing.

Orientation and position: 1 m above ground facing up

Energy: Energy (keV) as a function of channel is described by:

Energy = channel, 4096 channels

Resolution: The resolution (keV) varies with energy according to the function:

$$R(E) = \sqrt{2.45E}$$

3. Methods

For the PERLAD project, a series of experiments were carried out with a view towards a) investigating the efficiency of the detectors in the geometries as described previously and b) qualitative aspects of the use of $LaBr_3$ detectors for fresh fallout analysis. The determination of the efficiency of a detector for semi-infinite cloud geometries and semi-infinite slab geometries is a relatively difficult matter primarily because neither geometry is reproducible in real life for practicable direct calibration using sources. While analytical functions may be employed to estimate efficiency values, such approaches necessitate certain approximations and compromises. An alternative approach is the use of Monte Carlo based transport codes which, while at first glance appearing amenable to addressing the problem, also come with a series of intrinsic disadvantages. The main disadvantage being the length of time required to simulate photon transport through and over large volumes and areas. The small size of the detector relative to the volume or area over which a photon could possibly interact with it necessitates following a very large number of histories resulting in simulation times that are not practicable (weeks or months).

For the geometries being considered in the PERLAD project – direct measurement of airborne activity and direct measurement of ground deposited activity - the distances which must be considered are of importance. The transmission of gamma photons through air governs the volume and area respectively which the detector can be expected to “see” for various energies. The distances at which varying degrees of transmittance are experienced for a range of energies are depicted in Figure 6. Consideration of these distances indicates a number of problems with respect to simulation of a detector response for the two relevant geometries. For photons with energies of 1000 keV, there is still a significant chance (5%) of them reaching the detector out to distances of the order of 300 or 400 m, this distance being even higher for energies above that. A distance of 400 m corresponds to a hemispherical volume of approx. 1.38E+08 m^3. Given the relatively low efficiency of a small detector in this volume, the number of photons that would be required to be simulated per unit volume and the number seconds the detector would have to be assumed to be exposed for result in a cumulative number of histories to be simulated that exceeds

10^{12} or 10^{13}. For normal workstations this number of histories becomes prohibitively large with respect to the time necessary for the simulation.

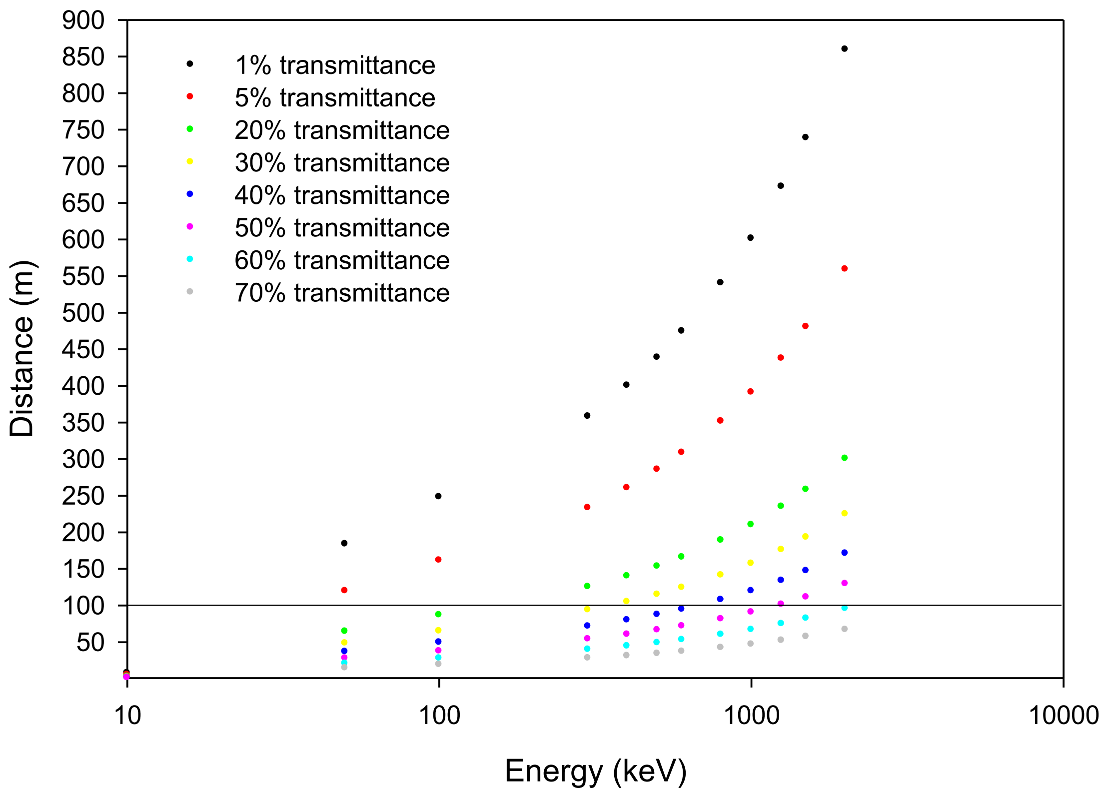

Figure 6. Transmission of photons of various energies through air as a function of distance.

For planar surface geometries, the problem is somewhat less with respect to the simulations but still significant with respect to the amount of time required to generate robust data.

It should be noted that for either of the geometries utilized, two aspects are of potential interest. The first of these is the photopeak and the second is the portion of the spectrum comprised of scattered radiation. While it is possible to generate data related to the photopeak efficiency for the geometries considered, consideration of the latter is more computationally difficult due to having to follow more histories through more complex matrices. For the former and for geometries such as semi-infinite clouds or surfaces, it is possible to restrict the number of histories followed by the simulation to only those that solely will interact with a defined volume around the detector. In this way, while the total number of histories generated remains the same, only those histories that follow a trajectory that would result in interaction with the defined target volume are followed. Consequently, the time required for simulation can be drastically reduced. This does however sacrifice a significant amount of information with respect to those histories that may not interact with the prescribed volume, but for which scattered radiation may contribute to the detector signal.

For the semi-infinite cloud geometry, a number of simulations were set up for mono-energetic photons being emitted within a hemispherical volume of air the radius of which corresponded to the distance at which less than 5% transmittance would be expected for the relevant photon energy (see Table 1). The detector model was the positioned at the center of the hemispheres base at a height and orientation corresponding to the detector description previously.

keV	**Hemisphere radius m**	**Total volume m^3**	**Activity per m^3**
60	204	1.78E+07	1000
100	250	3.27E07	543.34
200	310	6.24E+07	284.97
661	510	2.78E+08	64.0
1000	602	4.57E+08	38.91
1400	715	7.66E+08	23.23
2000	860	1.33E+09	13.35

Table 1. Hemispherical geometries employed of for assessment of efficiency values for direct cloud measurements.

For the semi-infinite slab geometry, a similar approach was followed and circular geometries with radii corresponding to 5 % transmittance for the relevant energies were established with the detector positioned at the correct height and with the correct orientation at the center of the disc (see Table 2). For the surface deposition simulations, the activity present (represented by mono-energetic photons) was either 1000 or 100 Bq/m^2.

keV	Disc radius m	Total area m^2
60	204	130740.4
100	250	196349.4
200	310	301906.8
661	510	817127.6
1000	602	1138524.8
1400	715	1606059.3
2000	860	2323520.0

Table 2. Circular geometries employed of for assessment of efficiency values for direct measurements of surface deposition.

For the purpose of the assessment of qualitative aspects of $LaBr_3$ detectors for nuclide assemblages typical of fallout situations a series of simulations were conducted for both cloud shine and surface deposition scenarios. For the former, a hemispheric volume of air with a radius of 70 m was employed and for the latter, a circular slab of radius 100 m was employed. Five scenarios in total were simulated: cloud activity 5-6 hours after the postulated release, cloud activity 20-21 hours after the postulated release, ground activities 3, 7 and 30 days after the postulated release. The isotopes and activities utilized for this aspect of the project were based on the work reported in Johansson et al. (2019). The following isotopes and activities were represented (see Tables 3 through 7, and Figures 7 through 10).

Isotope	Bq/m²	Area of circle m²	Total activity Bq
I-131	16202	31415.93	5.08998E+08
I-132	5945	31415.93	1.86778E+08
Te-132	5764	31415.93	1.81081E+08
Mo-99	5555	31415.93	1.74515E+08
Tc-99m	5364	31415.93	1.68502E+08
I-133	4026	31415.93	1.26481E+08
Cs-134	2860	31415.93	8.98496E+07
Ba-137m	1947	31415.93	6.11668E+07
Cs-136	560	31415.93	1.75898E+07
Sb-127	435	31415.93	1.36502E+07
Te-131m	288	31415.93	9.05407E+06
Te-129	278	31415.93	8.74420E+06
Ba-140	242	31415.93	7.60266E+06
La-140	159	31415.93	4.99011E+06
Sb-125	76	31415.93	2.37488E+06
Te-131	65	31415.93	2.04235E+06
I-135	21	31415.93	6.73872E+05
Br-82	17	31415.93	5.18363E+05

Table 3. Isotopes and activities for the 3 day ground deposition scenario.

Isotope	Bq/m²	Area of circle m²	Total activity Bq
I-131	20899	31415.93	6.56571E+08
Cs-134	5180	31415.93	1.62735E+08
I-132	4540	31415.93	1.42628E+08
Te-132	4420	31415.93	1.38858E+08
Mo-99	3680	31415.93	1.15611E+08
Tc-99m	3560	31415.93	1.11841E+08
Ba-137m	3520	31415.93	1.10584E+08
Cs-136	826	31415.93	2.59496E+07
Te-129m	738	31415.93	2.31850E+07
Ag-111	484	31415.93	1.52053E+07
Te-129	466	31415.93	1.46399E+07
Sb-127	384	31415.93	1.20637E+07
La-140	366	31415.93	1.15045E+07
Ba-140	354	31415.93	1.11212E+07
I-133	298	31415.93	9.36195E+06
Sb-125	137	31415.93	4.31010E+06
Ag-110m	64	31415.93	2.00434E+06
Te-131m	57	31415.93	1.79699E+06
Sn-125	47	31415.93	1.47655E+06

Table 4. Isotopes and activities for the 7 day ground deposition scenario.

Isotope	Bq/m²	Area of circle m²	Total activity Bq
Cs-134	5060	31415.93	1.5896461E+08
Ba-137m	3520	31415.93	1.1058407E+08
I-131	2855	31415.93	8.9694359E+07
Te-129m	460	31415.93	1.4451386E+07
Te-129	290	31415.93	9.1106564E+06
Cs-136	246	31415.93	7.7283188E+06
Sr-89	185	31415.93	5.8182302E+06
Sb-125	135	31415.93	4.2522090E+06
La-140	117	31415.93	3.6631588E+06
Ba-140	101	31415.93	3.1792921E+06
Ag-110m	60	31415.93	1.8786726E+06
Ag-111	57	31415.93	1.7907080E+06
I-132	31	31415.93	9.8646020E+05
Te-132	30	31415.93	9.5504427E+05
Rb-86	16	31415.93	4.9260178E+05
Mo-99	11	31415.93	3.4934514E+05
Sn-125	9	31415.93	2.8274337E+05
Sb-127	6	31415.93	1.9226549E+05
Sb-126	1	31415.93	3.5409910E+04

Table 5. Isotopes and activities for the 30 day ground deposition scenario.

Isotope	Bq/m³	Hemisphere volume m³	Total activity Bq
Xe-133	2.8E+04	718377.52	2.00643E+10
Xe-135	1.1E+04	718377.52	8.22183E+09
Kr-88	2.3E+03	718377.52	1.62425E+09
Rb-88	1.6E+03	718377.52	1.18329E+09
Kr-85m	1.4E+03	718377.52	9.95671E+08
Xe-133m	9.0E+02	718377.52	6.43666E+08
Xe-135m	6.4E+02	718377.52	4.60121E+08
Kr-87	2.7E+02	718377.52	1.91340E+08
I-133	1.7E+02	718377.52	1.22211E+08
I-132	1.4E+02	718377.52	9.90643E+07
Te-132	1.3E+02	718377.52	9.65499E+07
I-135	1.0E+02	718377.52	7.39210E+07
I-131	9.7E+01	718377.52	6.94174E+07
Cs-134	2.6E+01	718377.52	1.87066E+07
Mo-99	2.2E+01	718377.52	1.59157E+07
Ba-137m	1.8E+01	718377.52	1.26973E+07
Te-131m	1.7E+01	718377.52	1.21693E+07
I-134	6.2E+00	718377.52	4.46242E+06
Cs-136	5.9E+00	718377.52	4.22406E+06

Table 6. Isotopes and activities for the 5-6 hour cloud scenario.

Isotope	Bq/m³	Hemisphere volume m³	Total activity Bq
I-132	1.1710E+04	718377.52	8.4118E+09
I-133	1.1330E+04	718377.52	8.1392E+09
I-131	1.0142E+04	718377.52	7.2859E+09
Xe-133	9.5700E+03	718377.52	6.8749E+09
Xe-135	2.8490E+03	718377.52	2.0467E+09
I-135	2.3540E+03	718377.52	1.6911E+09
Cs-134	1.3420E+03	718377.52	9.6406E+08
Te-132	1.1440E+03	718377.52	8.2182E+08
Ba-137m	9.0750E+02	718377.52	6.5193E+08
Cs-136	2.9150E+02	718377.52	2.0941E+08
Sb-127	1.5400E+02	718377.52	1.1063E+08
Te-131m	1.1660E+02	718377.52	8.3763E+07
Xe-135m	4.6530E+01	718377.52	3.3426E+07
Te-131	2.6070E+01	718377.52	1.8728E+07
Rb-88	2.5960E+01	718377.52	1.8649E+07
Kr-88	2.0350E+01	718377.52	1.4619E+07
Ag-110m	8.7340E+00	718377.52	6.2743E+06

Table 7. Isotopes and activities for the 20-21 hour cloud scenario.

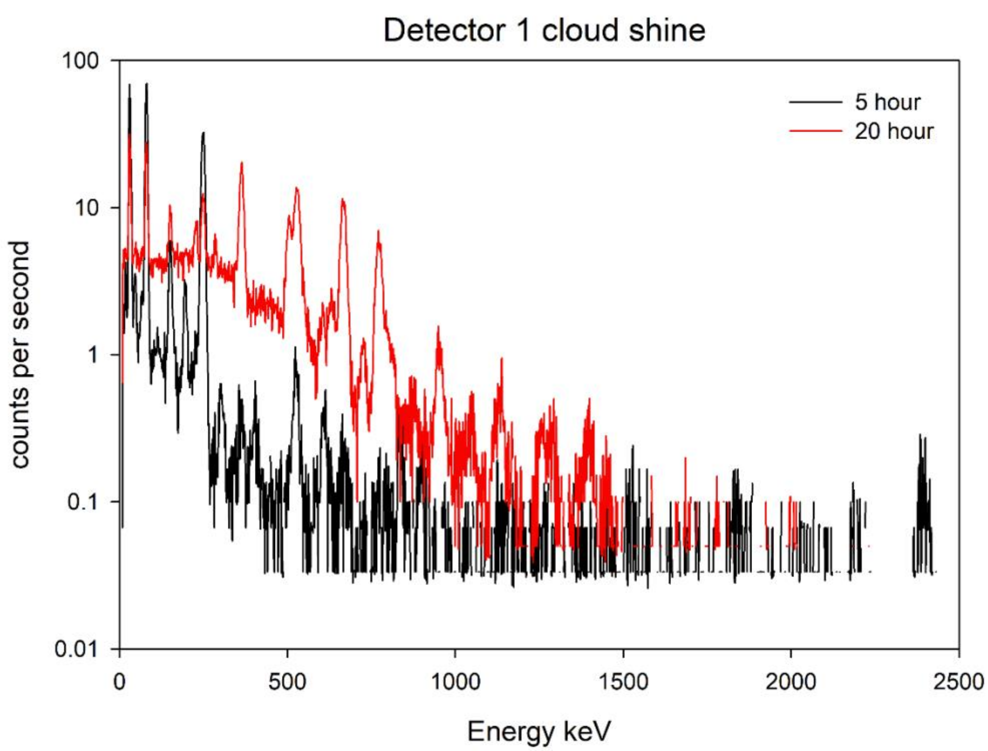

Figure 7. 5 hour and 20 hour cloud shine spectra for Detector 1.

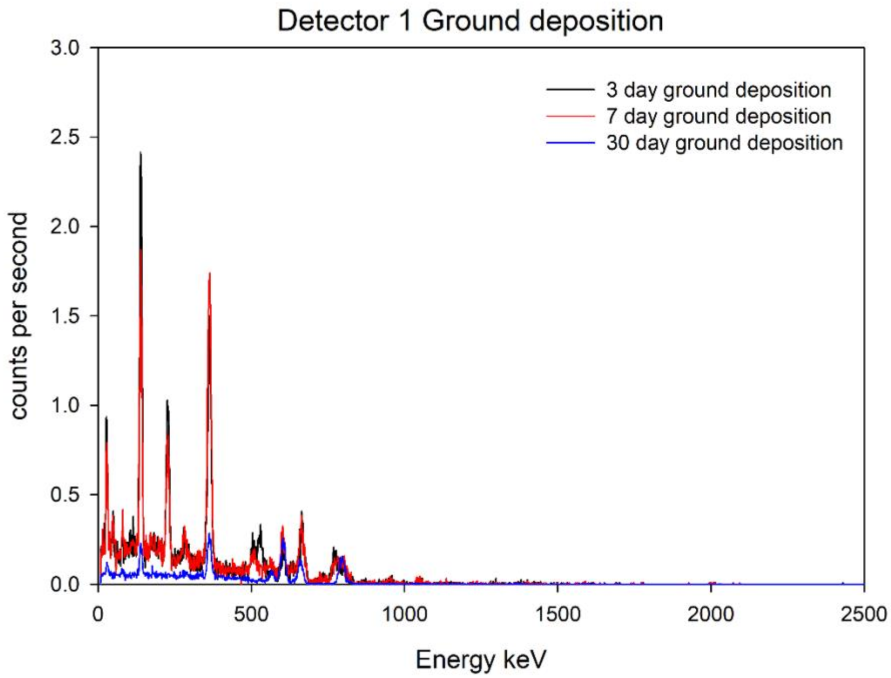

Figure 8. 3 day, 7 day and 30 day ground deposition spectra for Detector 1.

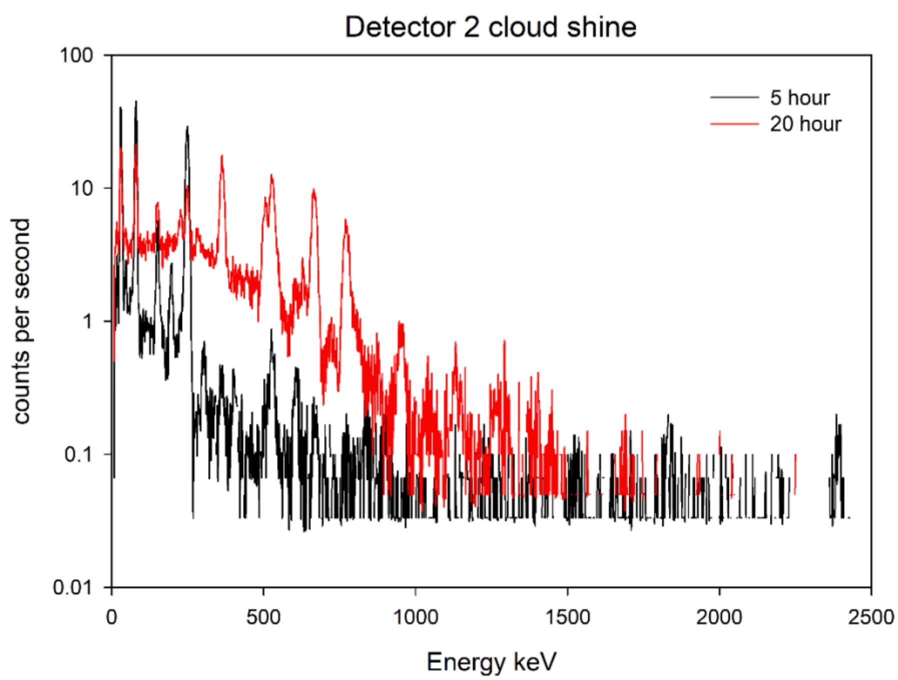

Figure 9. 5 hour and 20 hour cloud shine spectra for Detector 2.

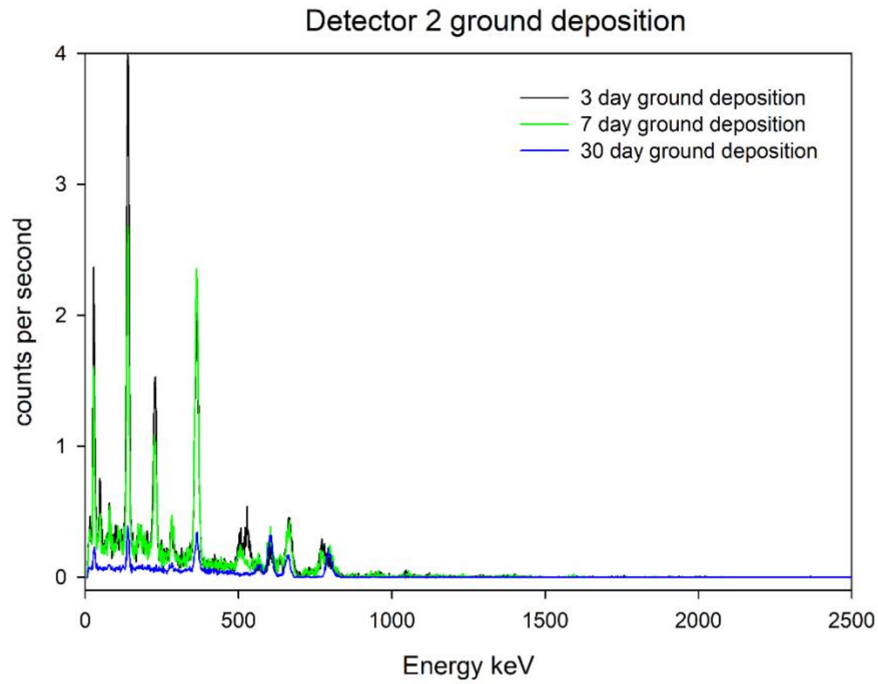

Figure 10. 3 day, 7 day and 30 day ground deposition spectra for Detector 2.

4. Simulations

All simulations were conducted with GEANT4 (Agostinelli et al, 2003). The physics packages QGSP_BIC_HP plus Radioactive Decay were employed throughout. Geometries were as described earlier in this text. Only histories that would interact with a 30 x 30 x 30 cm volume around the detectors were followed to completion. Despite this restriction, simulation times were still of the order of days for geometries corresponding to higher energies and data generated was in many cases unfit for purpose due to the low number of interactions with the detectors.

5. Results and Discussion

5.1 Cloud shine scenario - efficiency estimates

For the situation with respect to the efficiency of detectors placed in a semi-infinite contaminated cloud, a number of aspects proved problematic. For the $LaBr_3$ detectors (1 and 2), an initial model was constructed using the available information as to the construction of the detectors. These detectors, intended for use outdoors and "ruggedized" to some extent feature a number of constructional aspects not typically encountered in laboratory-based detectors including external weather proof shields, padding against impacts and integrated electronics. For the first attempt at assessing the detectors efficiency, the physical dimensions of the detectors, as provided for by the manufacturers were modelled and relatively generic compositional descriptions of constructional materials were used (i.e., standard compositions for plastic, expanded polystyrene, etc.). For the other detectors, in particular Detectors 3 and 5, large volumes of material are present such as cooling units, MCAs and associated structures and ruggedizing materials. In typical situations where a detector may be employed with the source in front of the detector unit, these materials have little or no impact on the signal. For situations such as those PERLAD concerns itself with, such materials may have significant impacts as proportions of the overall signal must pass through the entirety or parts of these structures depending on the incident angle of the photons. The construction of these aspects of the detector package are not described by manufacturers and are therefore, to large extent, impossible to model accurately based on the provided information. While the overall volume and mass can be determined, the internal homogeneity of the structures cannot be assessed, nor can accurate descriptions of the compositions be obtained. This places severe restrictions with respect to simulation of the detector response in a geometry where proportions of the signal will pass through these structures. In addition to uncertainties regarding the composition and construction of detector elements, there is an intrinsic difficulty in simulating radiation transport over large volumes with respect to the time required. For PERLAD, the upper limit set on time required was one week on a 16 core 4 GHz machine. As a result of this, for larger volume geometries it was the case that low counts were observed in the simulated spectra especially for the higher energies (larger volumes). This could be ameliorated to some extent by manipulation of the outputs such that the number of counts for the photopeak were more easily determined but the underlying problem remained for some of the detectors.

For Detectors 1 and 2 ($LaBr_3$ detectors in different configurations), the initial results are displayed in Figures 11 and 12. Results for Detectors 3 and 5 are displayed in Figures 13 and 14. Detector 4, CdZnTe, produced no meaningful results within the maximum time constraint for the simulations largely due to the small size of the detector relative to the volume being simulated. Cursory examination of the results for Detectors 1 and 2 indicate that the simulated peak efficiency is somewhat higher in the Detector 2 configuration. Assuming the data is reliable, a cause of this is in relation to the extra polyurethane foam protection present in the Detector 1 configuration. The extent to which this material may affect the efficiency values was investigated by changing the material density, polyurethane foam existing in a number of different forms depending upon the application (see Figures 15 and 16).

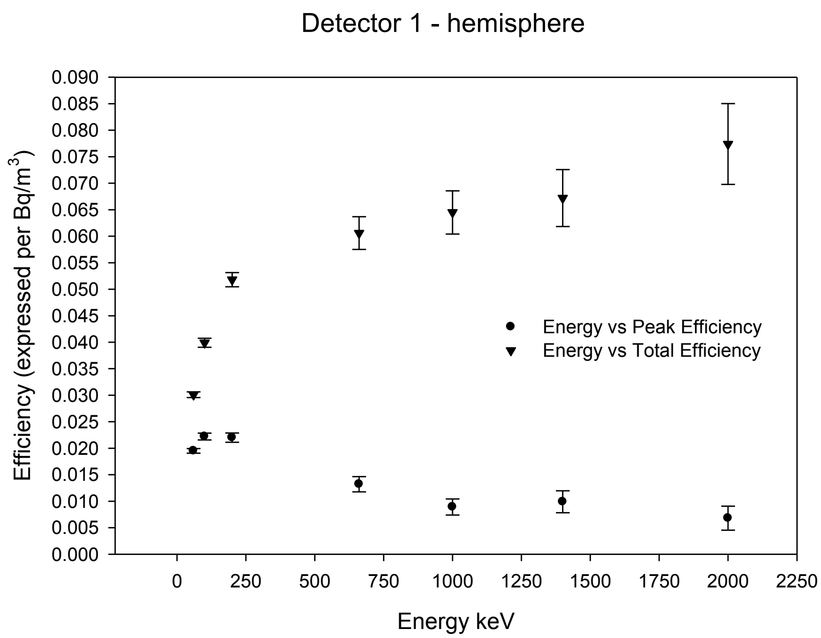

Figure 11. Efficiency curves for Detector 1 in the cloud shine scenario.

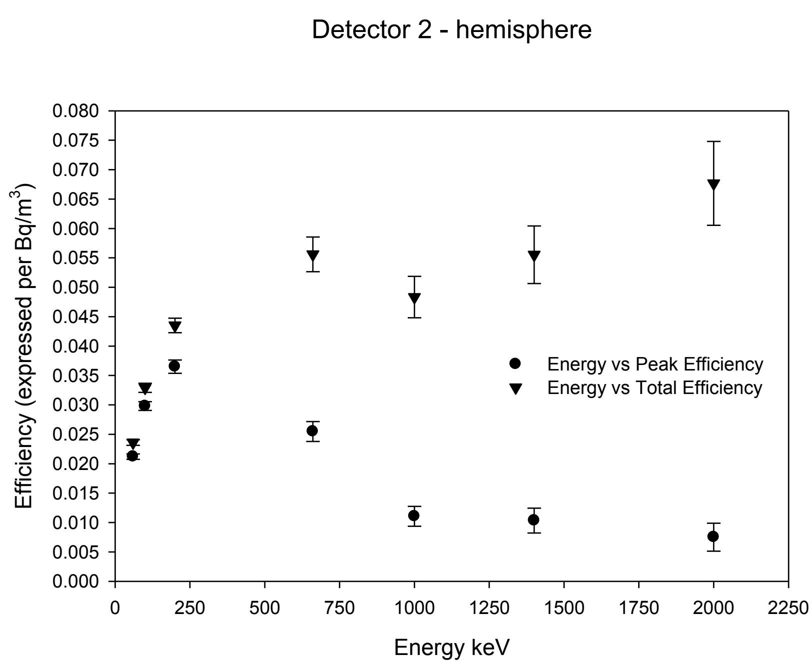

Figure 12. Efficiency curves for Detector 2 in the cloud shine scenario.

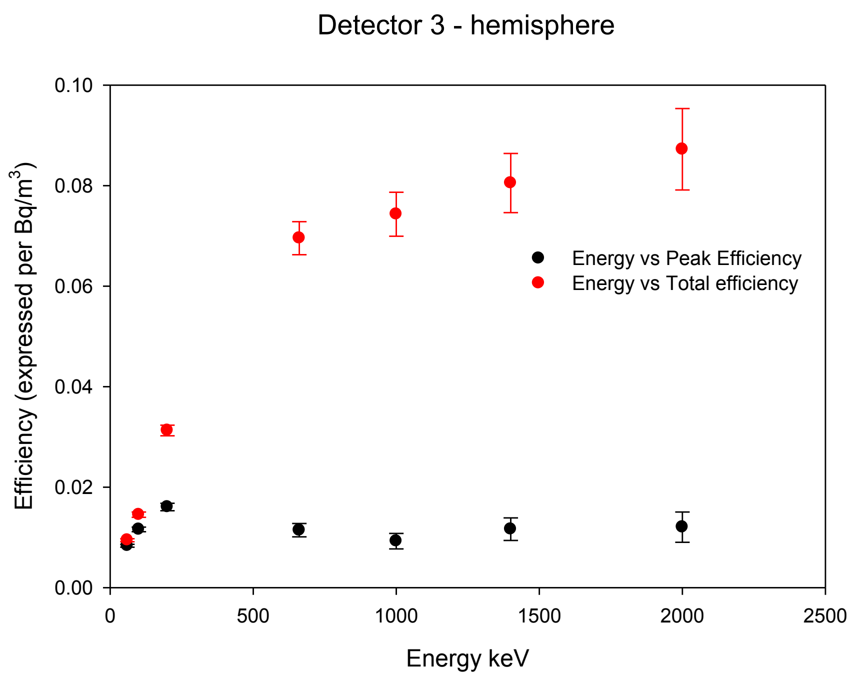

Figure 13. Efficiency curves for Detector 3 in the cloud shine scenario.

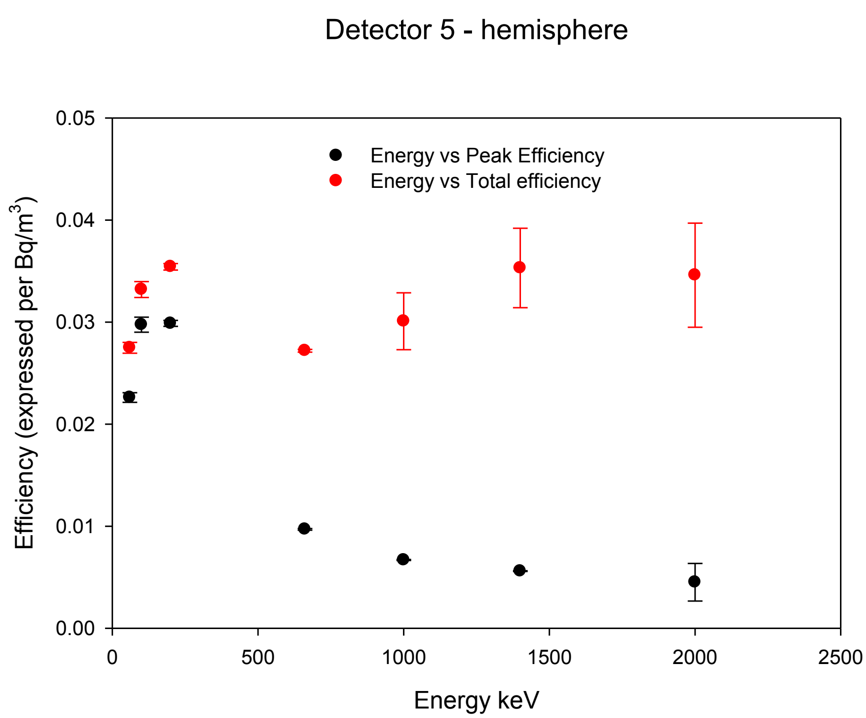

Figure 14. Efficiency curves for Detector 5 in the cloud shine scenario.

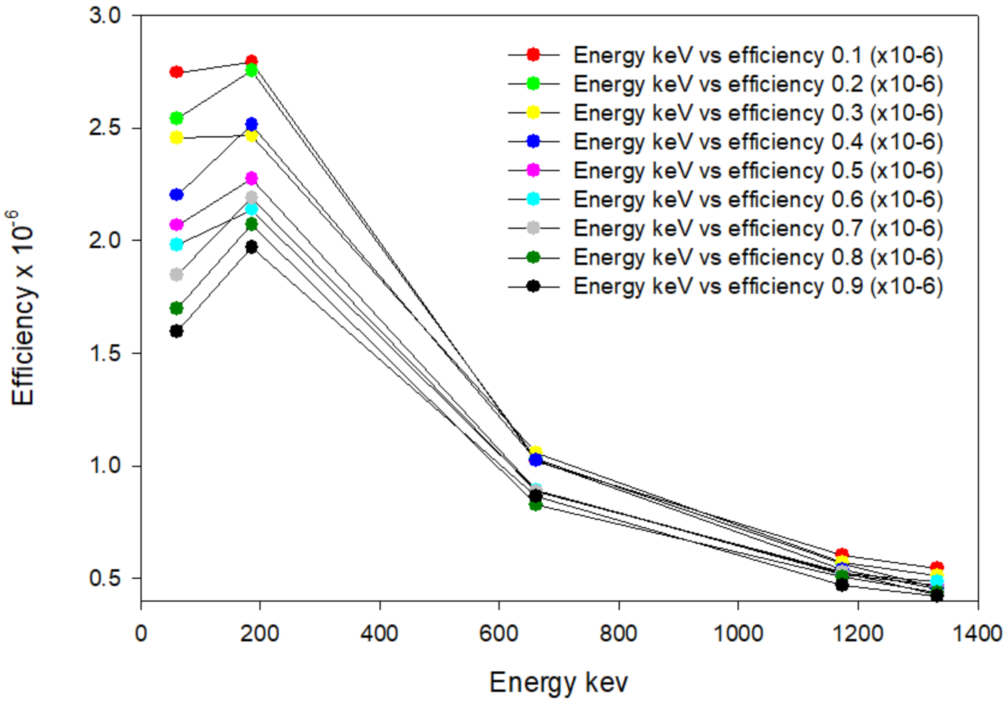

Figure 15. Impact of varying values of the density of polyurethane on the efficiency of Detector 1.

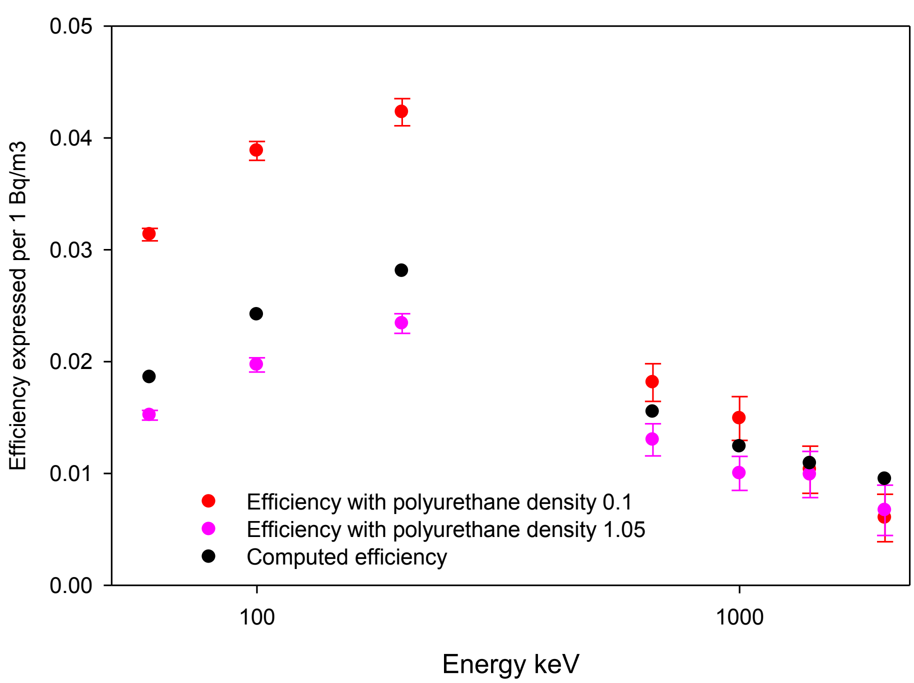

Figure 16. Computed efficiency of Detector 1 relative to two values of polyurethane density.

Figure 16 indicates that the density of the foam padding in Detector 1 is probably nearer to the greater values for density as opposed to the lighter forms of this material that are available. For the purpose of investigating further the extent to which the detector construction is impacting estimates of efficiency, a series of experiments were conducted with point sources for Detectors 2 and 3 in the laboratory – the $LaBr_3$ detector both with and without its weather shield and the HPGe Detective unit. For some parameters related to the detector construction, better information was made available over the course of the project over and above what was contained in the manufacturers' materials and this was incorporated into the models. The point sources were Co-60, Cs-137 and Am-241 sources (Fig. 17) and a Co-57 source. A small metallic sphere was present in the top of the plastic unit which was presumably the source, see Fig. 17. The nature of this sphere was unknown (solid, hollow, material, how the sources were distributed within it, etc.).

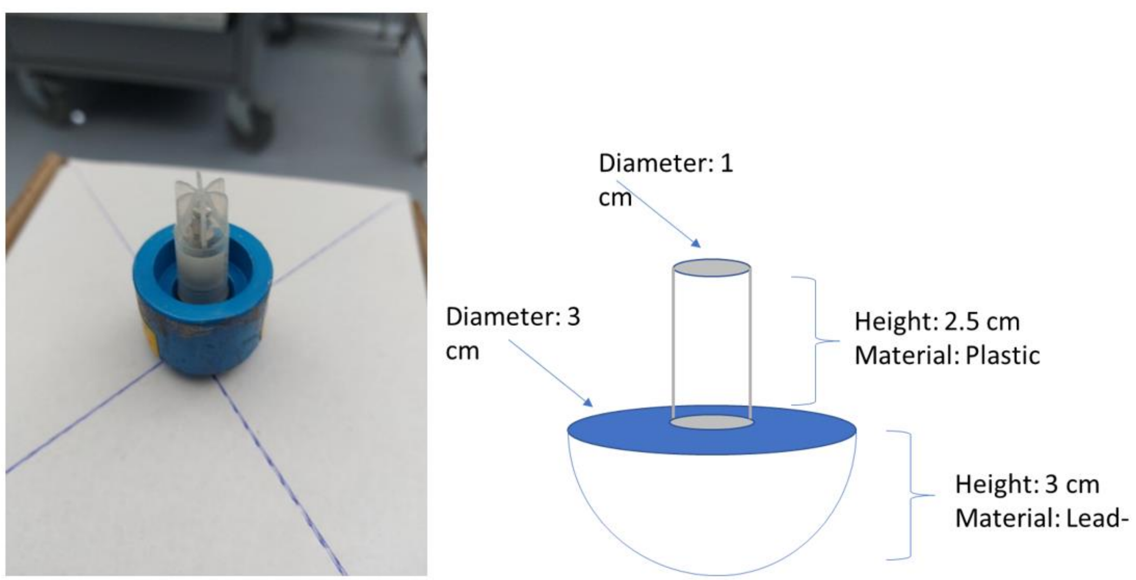

Figure 17. Mixed Am-241, Cs-137 and Co-60 source photo and schematic.

The Co-57 source was present as a small aluminium cylinder of approximately 1.5 cm in length and apparently of approximately 5 mm in diameter. How the source was present in this aluminium was unknown. Two options were therefore investigated: the source was homogenously distributed throughout a solid mass of aluminium or the source was only present on the outside (electroplated on for example) as a thin (0.001 cm) layer of aluminium around a solid aluminium cylinder. The actual experiments performed were conducted by positioning the sources in front of the two detectors at various distances and behind the detectors at the same distances, the reference point being the crystal centers (see Figure 18 and 19).

Figure 18. Detector 2 ($LaBr_3$) detector, measurement orientation front (left) and back (centre). Distance was measured to the center of the crystal. The detector was placed in an aluminum weather shield and the sources were measured in the front orientation (right).

Figure 19. Detector 3 (HPGe) measurement orientation front (left) and back (right). Distance is measured to the center of the crystal.

For the $LaBr_3$ detector (Detector 2) this process was repeated both with and without the aluminium weather shield. It was discovered that recent iterations of this detector do not actually have a polyurethane filler between this weather shield and the plastic detector housing, so this was emitted from the models. The distances were 2 m for Co-60 and Cs-137, 1.5 m for Co-57 and 1m for Am-241. For simulation purposes, "real" isotopes were simulated as opposed to mono-energetic sources. The live times for the real spectra were replicated in the simulations to allow for direct comparison of actual and simulated spectra. Data is presented in the following tables (Tables 9 and 10) which presents the counts recorded in the actual spectra in addition to the counts generated by a simulation for the same count time for both detectors. To check for consistency between the simulations, repeated simulations were run for two setups: Cs-137 and Co-60, 2 m in front of the unshielded Detector 2 and Am-241 in front of Detector 2 both with and without shield. Results are displayed in Table 8.

For the $LaBr_3$ detector, medium to high energies present no significant problems for sources being measured in front of the detector – it is a relatively simple geometry and there are limited variables to take account of. The presence of unknown structures or materials within the aluminium endcap is probably not an issue. The model performs well for both Cs-137 and Co-60 irrespective of which orientation the source is coming from. Both isotopes yield results that would be usable for the intended purpose. The results indicate that the presence of the weather shield is of less import than other aspects of the detector which are not being addressed or are being addressed in an incorrect way by the model. These aspects are most likely related to components of the construction of the detector and the materials used.

For low energies (< 200 keV) the deficiencies in the model are evident with little correspondence between the modelled detectors and the actual detectors. For both Co-57 and Am-241, indications are that the front of the detector is not being modelled correctly, the actual detector exhibiting a greater level of shielding than the model from the front and less than the model from the rear. For signals from behind the detector the matter is less simple given the materials present in the MCA/PMT unit. Tables 9 and 10 provide data related to directional measurements conducted on both Detectors 2 and 3. For Am-241 and Detector 2, with the source behind the detector, no simulated signal could be observed for the count times employed despite evident signals in the actual spectrum. It is most probable that there is an issue with respect to how the rear aspects of the detector unit are constructed – the model assumes homogenous structures of certain compositions and density and while these may accord with the mass and volume of the actual detector unit, it is impossible to ascertain the homogeneity of the rear structures of the actual detector. It is possible that there exist voids or channels with less shielding and these may not be represented in the model.

Run	661 keV area	1172 keV area	1332 keV area	59 keV with shield	59 keV no shield
1	7273	5932	5074	75547	75152
2	6927	5780	5064	75140	73474
3	6874	5748	5129	74751	70618
4	6874	5585	5124	75139	75011
5	6851	5903	5019	75387	75202
6	6896	5799	5124	74790	75411
7	6846	5831	5067	75401	75245
8	6936	5839	5015	75291	75389
9	7090	5801	5232	75258	75064
10	6838	5712	5062	75476	74692
Average	6940	5793	5091	75218	74526
SD	138 (1.98 %)	98 (1.7 %)	64 (1.25 %)	270 (0.3 %)	1484 (1.2 %)
Actual value	7055	5373	4894	22181	23744

Table 8. Repetitions of simulations for Cs-137 and Co-60 2 m from the front of Detector 2 without weather shield and Am-241 1 m in front of Detector 2 both with and without shield.

Bearing that in mind, it is difficult to see how accurate measures of efficiency could be obtained using simulations for the HPGe detector for the cloud shine scenarios as, for the configuration presented (where it is facing downwards), most of the signal will be arriving through the electronics unit. A possible alternative to scanning the detector would be a very comprehensive regime of very carefully performed measurements with a specific type of point source (where the source housing plays no role). For the HPGe detector (Detector 3), the situation is even more complex. Even for situations where the source is coming from the front the results are relatively poor even for higher energies. The dimensions of the crystal from the manufacturer are “nominal”, there is no information as to what is surrounding the detector within its housing (there may be support structures, housing etc.), there is no information as to dead layers or the position of the crystal with respect to any of the three possible axes (tilting, not central etc.).

Nuclide	Act. (MBq)	Dist. (m)	E (keV)	Orient.	Livetime (s)	Area Simulated	CPS Simulated	Area Actual	CPS Actual
Am-241 as «pure point» source	10.7	1	60	Front	260	74526 ± 1484 *	286	23744	89
				WS	269	75218 ± 270*	279	22181	83
				Back	892	?????	????	1131.6	1.27
Am-241 as aluminium point source	10.7	1	60	Front	260	69410	266	23744	89
				WS	269	81071	301	22181	83
				Back	892	??????	????	1131.6	1.27
Co-57 as volume source	10.4	1.5	122	Front	372	92490	248	80177	216
				WS	375	91488	244	87220	237
				Back	428	97	0.22	8145	19.0
			136	Front	372	11634	31.3	4144	11.1
				Back	428	47	0.10	330	0.77
Co-57 as a thin surface source	10.4	1.5	122	Front	372	30925	265	80177	216
				WS	375	97679	260	87220	237
				Back	428	327	0.76	8145	19.0
			136	Front	372	3684	33.3	4144	11.1
				Back	428	121	0.28	330	0.77
Cs-137	8.9	2	662	Front	156	6940 ± 138*	44.7	7055	45.2
				WS	248	10787	43.5	11096	44.7
				Back	280	4314	15.40	4847	17.3
Co-60	3.5	2	1173	Front	503	5792 ± 98*	11.6	5373	10.7
				WS	491	5309	10.81	5850	11.9
				Back	500	2612	5.22	2757	5.5
			1332	Front	503	5091 ± 64*	10.28	4894	9.7
				WS	491	4674	9.51	5073	10.3
				Back	500	2482	4.96	2602	5.2

Table 9. Comparison of real and simulated spectra for the $LaBr_3$ detector (Detector 2). WS denotes the presence of the aluminium weather shield, * denotes values based on 10 replicates. Uncertainties where presented are 1 sigma.

Nuclide	Act. (MBq)	Dist. (m)	E (keV)	Orient.	Livetime (s)	Peak area Simulated	CPS Simulated	Peak area Actual	CPS Actual
Am-241	10.7	1	60	Front	216.5	92250	426	6427.5	30
				Back	1230	129	0.1	0	0
Co-57 as volume source	10.4	1.5	122	Front	160.4	56629	353	44439	277
				Back	1315	39607	30.1	1632.5	1.2
			136	Front	160.4	6856	42.85	5940	37
				Back	1315	6217	4.7	375.0	0.29
Cs-137	8.9	2	662	Front	137.2	7215	52.6	5880.4	43
				Back	469.7	8950	19	1079.5	2.3
Co-60	3.5	2	1173	Front	315.4	4496	14.25	3504.4	11
				Back	391.1	2573	6.5	316.1	0.8
			1332	Front	315.4	3994	12.6	3036.0	9.6
				Back	391.1	2342	5.9	345.1	0.88

Table 10. Comparison of real and simulated spectra for the HPGe detector (Detector 3).

For sources placed to the rear of the detector, the electronics unit is a total unknown aside from overall volume and mass. The model used the weight of the box and its volume to arrive at an average density which is a very crude approach and is probably not good enough – the real instrument contains a battery, a cooling unit, a wide variety of circuitry units and probably a large number of void spaces. It appears that the average density approach to this structure is resulting in severe overestimation of transmission even at high energies. From the front, for high energies, crude estimates of efficiency are possible but would not represent useable data.

The implications of these experiments for consideration of the Monte Carlo modelling approach for calibration of these detectors for direct measurement of airborne activity is relatively clear. For simple detector geometries – Detectors 1,2 and 5 – it is probable that adequate estimates of efficiency at energies in excess of 400 keV can be obtained using relatively crude models. Results indicate that irrespective of the direction, the response of the detector can be modelled such that reasonable estimates of efficiency can be obtained. This is not the case for energies lower than about 400 keV.

It should be noted that even if the detector model could be improved with respect to the crystal and its housing, it is unlikely that the rear parts of the housing – through which a significant amount of the signal would pass for a cloud shine scenario – could be modelled accurately enough to ensure reliable data for lower energies without a complete dismantling of the detector or at the very least, a rigorous campaign of x-ray analysis or CT scanning to elucidate the inner structures of the detector unit.

With respect to the results generated for the cloud shine scenario, it is probable that for energies above 400 keV these are relatively reliable for Detectors 1,2 and 5 but in no way reliable for Detector 3. As noted above, improvements to the situation for Detectors 1, 2 and 5 could probably be obtained but it is doubtful that the situation regarding Detector 3 could be improved in any meaningful way.

Comparison with data from other work is difficult due to a relative lack of information as to $LaBr_3$ detectors employed for the purposes described in PERLAD. An obvious comparison is to that of Urban and Vágner (2019) and it appears that the data for Detector 2 (See Figure 12) which is the configuration most resembling that employed in their work, is somewhat comparable. The lowest energy considered in that work appears to be 200 keV and the value they determine appears relatively similar to that in Figure 12. Higher energies are similar. This however cannot be relied on as a robust comparison as there is no evidence in their work of any validatory measurements having been carried out nor is there any information as to how their simulation is conducted (with respect to the parameters employed).

5.2 Surface Deposition

For the estimation of peak efficiency for the different detectors with respect to surface deposited activity, a similar procedure was carried out as for the cloud shine scenarios. The radii of the disks at various energies corresponded to those employed for the hemispherical geometries, the detectors being positioned centrally and at the heights and orientations as described earlier in the report. A summary of peak efficiency values is displayed in Figure 20.

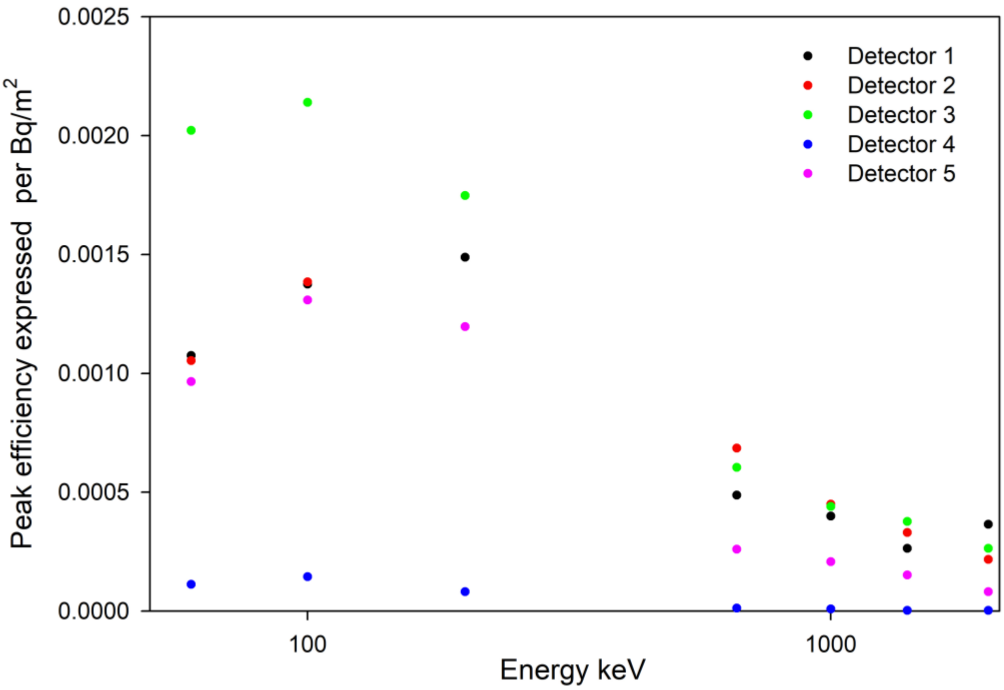

Figure 20. Peak efficiency data derived from Monte Carlo simulations for the five detectors for surface deposition.

Although the data derived from simulation was subject to the same problems as for the hemispherical geometries, some general trends can be discerned. Both Detectors 1 and 2 have similar values for peak efficiency. The HPGe detector (Detector 3) exhibits a higher apparent efficiency that either of the $LaBr_3$ detectors most probably being due to the lower amount of shielding around the crystal due to the construction of the detector assemblies. The NaI detector (Detector 5) is comparable to both the $LaBr_3$ configurations whilst the CdZnTe detector failed to provide meaningful data over the energy range and under the conditions of the simulation. As for the hemispherical geometries, the necessity to simulate photon transport over exceedingly large distances for the higher energies is a distinct disadvantage for a Monte Carlo approach to estimating efficiency. Combining this with a lack of information as to structural elements leads to a situation where uncertain data is generated over impracticable time periods.

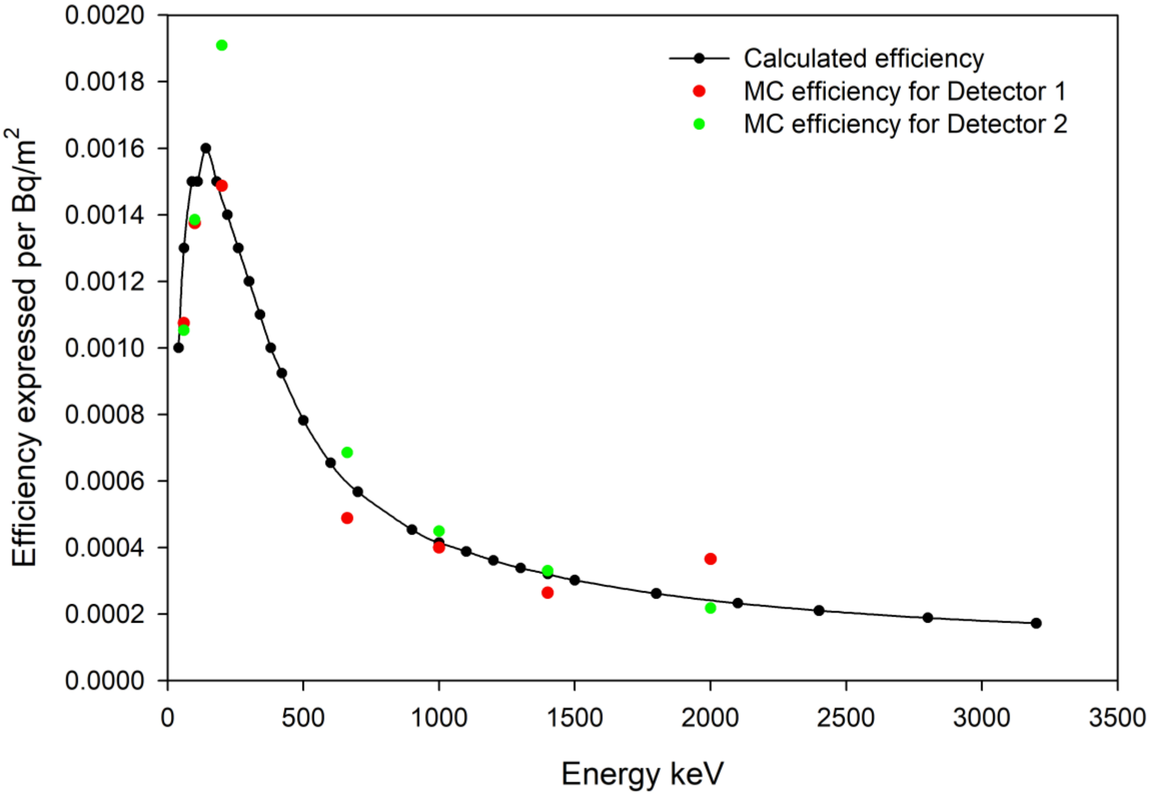

Figure 21. Peak efficiency data derived from Monte Carlo simulations for the two $LaBr_3$ detectors for surface deposition as compared with efficiency data derived as in Toivonen et al (2009).

5.3 Qualitative analysis

Three different software were used to analyze the spectra detailed in Section 3 previously. The objectives were to:

- Identify the nuclides contributing to the spectrum
- Determine the activity concentrations of the identified nuclides

The software and their uses were:

- Unisampo – gamma spectroscopy software written for germanium detectors. The automatic identification capability was tested.
- JMufi – peak based gamma spectrum analysis. The capability to identify nuclides was tested.
- Spectrum tool – a gamma spectroscopy toolkit written for low resolution detectors. Automatic identification, manual analysis and activity calculation were tested.

Each software has an automatic identification capability based on a preselected set of nuclides deemed appropriate. The selection of nuclides represents the emphasis of each software, e.g. for Spectrum tool the emphasis is security use (with nuclides such as Pu-239, U-235 and various medical bare and shielded sources in its library), whereas for JMufi the emphasis is on environmental monitoring (with typical fission products one might expect in a nuclear accident).

The capabilities of doing manual analysis are very different among the software. In JMufi there is no manual analysis capability, this software is used as an automatic processor of spectra incoming from the spectrometers of the national dose rate monitoring network. In Unisampo peaks can be added to or removed from the analysis, the identifications and activity concentrations will then reflect the combination of peaks in the analysis. In Spectrum tool nuclides and their responses are added to the analysis by the user.

The simulated spectra didn't contain the contribution of natural background, which makes the analysis process easier than it would be under actual circumstances. Additionally, in the simulated spectra, the energy calibration was better than it would be under real circumstances. The simulated spectra do not display the effects caused by slight fluctuations of the energy calibration that is often exhibited in environmental *in-situ* spectra.

5.4 Overview of identification results

Some nuclides contributing to the spectra were identified by the automatic identification algorithms of each software. Each software also produced false identifications. The false identifications are, however, not important in environmental application as no action is likely to be triggered based solely on the result of the automatic analysis. In this application, manual analysis capability is important. When the resulting spectra are complex, the automatic capabilities are likely to produce false identifications. The correct identifications of the automatic identification algorithms provide starting points for manual analyses. On manual analysis, the spectrum was explained well in each case starting from the nuclides suggested by the automatic analyses.

Unisampo (mainly geared towards Germanium spectrometry) produced very good automatic identification results once calibrations were established and analysis parameters were adjusted. Default analysis parameters did not produce good results. Working with calibrations is difficult in this software, it is clearly meant to have a static set of calibrations that is rarely altered. This is usually not the case in environmental spectroscopy, instead, it is important to be able to recalibrate any spectrum quickly.

5.5 Overview of quantification results

Quantitative results (deposition densities and airborne concentrations) were calculated for four of the most prominent nuclides in each measurement using Spectrum Tool. The results are given in Tables 11 through 15 below.

Nuclide	Deposition density (Simulated) (kBq/m^2)	Deposition density (Detector 1) (kBq/m^2)	Deposition density (Detector 2) (kBq/m^2)
I-131	16.202	13.98	18.83
I-132	5.945	4.01	6.0
Te-132	5.764	5.03	7.6
Mo-99	5.555	5.12	5.12

Table 11. 3-day ground deposition results provided by Spectrum Tool.

Nuclide	Deposition density (Simulated) (kBq/m^2)	Deposition density (Detector 1) (kBq/m^2)	Deposition density (Detector 2) (kBq/m^2)
I-131	20.899	16.89	22.7
Cs-134	5.180	3.5	4.45
I-132	4.540	2.59	4.01
Te-132	4.420	3.74	5.67

Table 12. 7-day ground deposition results provided by Spectrum Tool.

Nuclide	Deposition density (Simulated) (kBq/m^2)	Deposition density (Detector 1) (kBq/m^2)	Deposition density (Detector 2) (kBq/m^2)
Cs-134	5.060	3.72	5.15
Cs-137	3.520	2.54	3.36
I-131	2.855	2.76	3.25
Te-129m	460	-	-

Table 13. 30-day ground deposition results provided by Spectrum Tool.

Nuclide	Activity conc. (Simulated) (kBq/m^3)	Activity conc. (Detector 1) (kBq/m^3)	Activity conc. (Detector 2) (kBq/m^3)
Xe-133	28	33.97	25.95
Xe-135	11	10.74	9.64
Kr-88	2.3	2.71	1.93
Rb-88	1.6	1.21	1.21

Table 14. 5-hour cloud results provided by Spectrum Tool.

Nuclide	Activity conc. (Simulated) (kBq/m^3)	Activity conc. (Detector 1) (kBq/m^3)	Activity conc. (Detector 2) (kBq/m^3)
I-132	11.71	7.4	7.07
I-133	11.33	8.01	7.04
I-131	10.14	8.07	6.16
Xe-133	9.57	9.49	7.09

Table 15. 20 hour cloud results provided by Spectrum Tool.

The peak areas determined by UniSampo were very similar to Spectrum Tool, so using the appropriate peak efficiency calibration would yield a similar result. The peak efficiency calibrations used for the result are based on the computational method described in Toivonen (2009). The efficiencies are given in Table 16. Both Detector 1 and 2 used the same calibrations, both derived from a 5 meter point source FEPE calibration for unpackaged 1.5” $LaBr_3$(Ce) detector.

Energy (keV)	Full energy peak efficiency cloud	Full energy peak efficiency deposition
20.0	0.00137	2.4421e-5
40.0	0.01196	0.0010
60.0	0.01862	0.0013
90.0	0.02330	0.0015
110.0	0.02513	0.0015
140.0	0.02699	0.0016
180.0	0.02820	0.0015
220.0	0.02789	0.0014
260.0	0.02656	0.0013
300.0	0.02514	0.0012
340.0	0.02342	0.0011
380.0	0.02194	0.0010
420.0	0.02060	9.236e-4
500.0	0.01843	7.818e-4
600.0	0.01635	6.538e-4
700.0	0.01487	5.670e-4
900.0	0.01303	4.536e-4
1000.0	0.01240	4.140e-4
1100.0	0.01200	3.875e-4
1200.0	0.01156	3.606e-4
1300.0	0.01119	3.380e-4
1400.0	0.01090	3.199e-4
1500.0	0.01059	3.015e-4
1800.0	0.00984	2.615e-4
2100.0	0.00932	2.322e-4
2400.0	0.00886	2.102e-4
2800.0	0.00850	1.881e-4
3200.0	0.00826	1.720e-4

Table 16. Peak efficiency values for two configurations for an unpackaged 1.5” $LaBr_3(Ce)$ detector derived from a 5 meter point source calibration as detailed in Toivonen et al (2009).

The cloud analyses were all pretty much similar. Two examples are given below.

Example 1: 20_hour_cloud_detector2.Chn

Automatic identification (SpectrumTool):

Nuclide Identification: Bi-212

Category: NORM - Naturally occurring nuclide

ConfidenceClass: 4

Class description:

Two peaks

Info:

Characteristic line(s):

727.3 keV present with signf.:0.46

Additional lines(s):

1679.7 keV present with signf.:0.56

1073.6 keV absent with signf.:0.0

Nuclide Identification: Cs-137

Category: IND - Industrial usage nuclide

ConfidenceClass: 3

Class description:

Unequivocal peak

Info:

The presence of Am-241, I-131 was excluded

Characteristic line(s):

661.7 keV present with signf.:3.7

Nuclide Identification: I-123[sh]

Category: MED - Medical usage nuclide

ConfidenceClass: 1

Class description:

Small peak

Info:

The presence of I-123 was excluded

Characteristic line(s):

535.5 keV present with signf.:1.43

Nuclide Identification: I-132

Category: IND - Industrial usage nuclide

ConfidenceClass: 7

Class description:

Three or more peaks, two of them unequivocal

Info:

Characteristic line(s):

667.71 keV (yield=98.7%) present with signf.:5.37

772.6 keV (yield=75.6%) present with signf.:3.77

954.55 keV (yield=17.5%) present with signf.:1.29

522.65 keV (yield=15.9%) present with signf.:0.99

Suggestion: I-131

ConfidenceClass: 0

Class description:

Inconclusive identification

Info:

Characteristic line(s):

364.48 keV (yield=81.5%) present with signf.:4.52

Additional lines(s):

636.98 keV (yield=7.1%) absent with signf.:0.0

284.3 keV (yield=6.1%) present with signf.:0.45

80.18 keV (yield=2.6%) present with signf.:4.42

Automatic identification (Unisampo)

Unisampo identification result was very good:

UniSAMPO 2.72 (1 Apr 2019) Copyrighted 2022-Jan-05 10:30:35

License: Lic. no. 20050608-1, STUK/TKO Helsinki, Finland.

******** R A D I O N U C L I D E   A N A L Y S I S   R E P O R T *********

Un det set	Nuc lid #	Nuclide name	Confid	Activity	Activity uBq/m3	Activity Bq(ccorr)	Error Bq
76	1	Kr-85m	0.72	0.000	0.000	1300.560	12.44
3	2	I-131	0.81	0.000	0.000	7464.809	10.10
13	3	I-132	0.72	0.000	0.000	6408.412	5.85
87	4	I-133	0.87	0.000	0.000	8935.512	9.33
23	5	I-135	0.11	0.000	0.000	1018.675	14.42
92	6	Xe-135	0.97	0.000	0.000	26012.611	13.01

Automatic identification (JMufi)

comments	lineEnergy	nuclideId	significance
Ilma	80.9971	Ba-133a	4.892328765381738
Ilma	80.9971	Xe-133	4.892328694405487
Ilma	364.498	I-131a	8.72340391795482
Ilma	511	Annihilati	1.2381190318357682
Ilma	537.261	Ba-140	1.7996735801866226
Ilma	636.989	I-131b	1.02938869643369
Ilma	661.657	Cs-137	5.452487258276989
Laskeuma	80.9971	Ba-133a	4.89232876538174
Laskeuma	80.9971	Xe-133	4.89232869440549
Laskeuma	364.498	I-131a	8.72340391795482
Laskeuma	511	Annihilati	1.23811903183577
Laskeuma	537.261	Ba-140	1.79967358018662
Laskeuma	636.989	I-131b	1.02938869643369
Laskeuma	661.657	Cs-137	5.45248725827699

+----------+------------+------------+--------------------+

Manual analysis (SpectrumTool)

Nuclides in the spectra were determined to be

I-131

Te-132

I-132

I-132m

I-133

Xe-133

Cs-134

I-135

Xe-135

Cs-137

Comments

This spectrum was the first to be analyzed. Spectrum Tool software was used. The spectrum is quite well explained by the nuclides in the manual analysis. The key findings from the automatic identification are the presence of I-131 and I-132 and Cs-137. This would suggest more nuclides to try

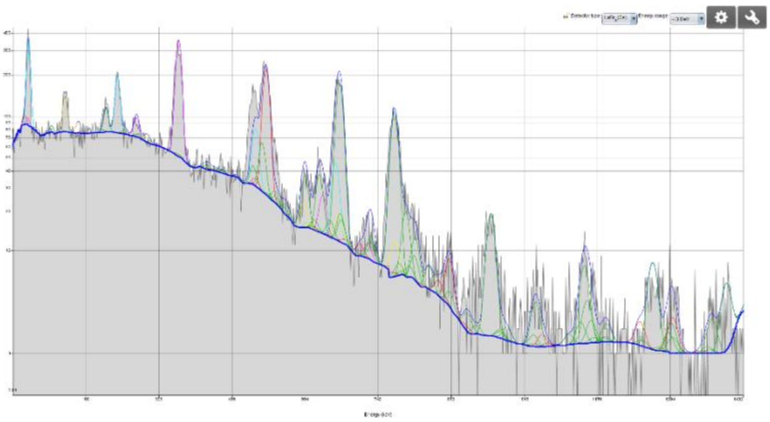

(such as I-133, I-132M, Xe-133, I-135, Xe-135 and Cs-134).

Some peak areas were left without explanation (around 505 keV and 547 keV):

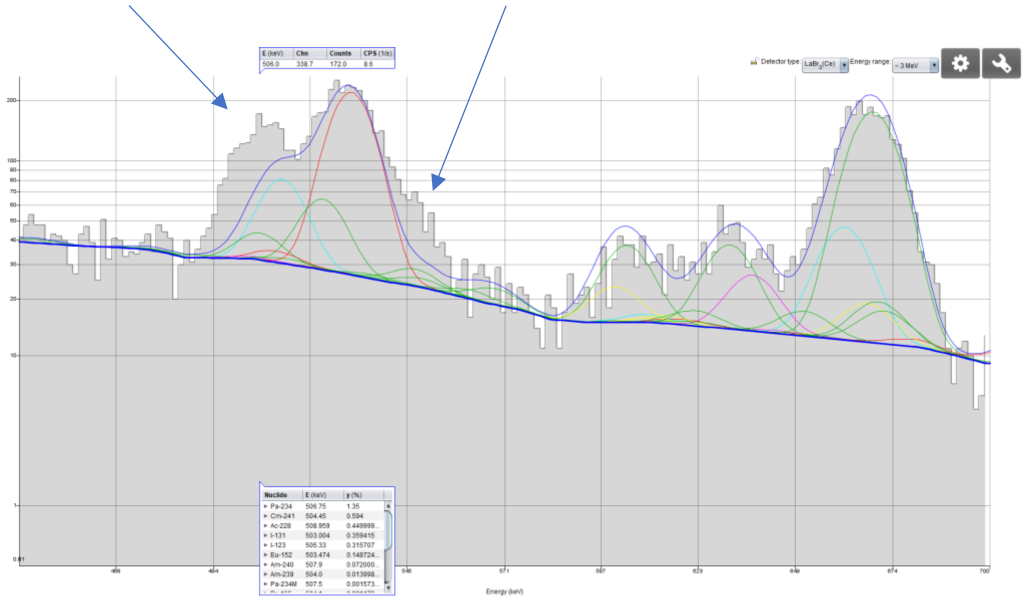

Most of the nuclides could be placed into the response quickly, in about 15 minutes. The attempt to explain the area near 510 keV then took over an hour, at which point the attempt was abandoned.

Example 2: 5_hour_cloud_detector1.Chn

The cloud spectra were analysed after 20_hour_cloud_detector2.Chn spectrum. The automatic identifications of I-132m and Kr-88 prompted the attempt of placing isotopes of Iodine and Krypton into the spectrum. The isotopes of Xenon also follow from the iodine parent. Cesium isotopes can then be attempted.

Automatic identification (Spectrum Tool)

Nuclide Identification: Bi-214

Category: NORM - Naturally occurring nuclide

ConfidenceClass: 1

Class description:

Small peak

Info:

Characteristic line(s):

609.3 keV (double peak) present with signf.:1.72

Additional lines(s):

1764.5 keV absent with signf.:0.03

1120.3 keV absent with signf.:0.22

Nuclide Identification: I-123[sh]

Category: MED - Medical usage nuclide

ConfidenceClass: 1

Class description:

Small peak

Info:

The presence of I-123 was excluded

Characteristic line(s):

535.5 keV present with signf.:0.76

Nuclide Identification: I-132M

Category: IND - Industrial usage nuclide

ConfidenceClass: 5

Class description:

Two peaks, at least one clear

Info:

Characteristic line(s):

599.79 keV (yield=14.0%) present with signf.:0.64

772.6 keV (yield=13.9%) present with signf.:0.5

667.71 keV (yield=13.9%) present with signf.:0.8

Additional lines(s):

175.0 keV (yield=8.8%) absent with signf.:0.0

Nuclide Identification: Kr-88

Category: IND - Industrial usage nuclide

ConfidenceClass: 5

Class description:

Two peaks, at least one clear

Info:

Characteristic line(s):

2392.11 keV (yield=34.5%) present with signf.:1.34

196.3 keV (yield=25.9%) present with signf.:2.22

2195.84 keV (yield=13.1%) present with signf.:0.54

834.83 keV (yield=12.9%) present with signf.:0.6

Automatic identification (Unisampo)

```
UniSAMPO 2.72 (1 Apr 2019) Copyrighted 2022-Jan-05 10:37:40

License: Lic. no. 20050608-1, STUK/TKO Helsinki, Finland.

********  R A D I O N U C L I D E    A N A L Y S I S    R E P O R T  *********


Un Nuc Nuclide Confid      Activity       Activity       Activity Error

det lid    name              uBq/m3             Bq     (ccorr) Bq

            set  #


96   1 O-19     0.31          0.000          0.000        552.434 30.07

100   2 Ge-71m  0.82 1310057600.000       1310.058        915.518 11.27

76   3 Kr-85m   0.99          0.000          0.000       2274.587 11.02

50   4 Kr-87    0.39          0.000          0.000        388.504 15.50

26   5 Kr-88    0.36          0.000          0.000       1931.244 13.89

94   6 Y-88     0.87 50463856656384.000   50463856.000    236.536 20.81

7   7 Te-125m  0.93 770389270695205928960.000 770389290516480.000   96649.375  10.54

7   8 I-125    1.00 361357328810535550976.000 361357341884416.000   97971.312  10.54

3   9 I-131    0.60          0.000          0.000          104.761  26.59

16  10 I-132    0.05          0.000          0.000        222.022  15.15

92  11 Xe-135   0.98          0.000          0.000      15222.242  14.23

4  12 Pb-210   1.00 31041939456.000      31041.939      26434.396  11.60
```

Manual analysis (Spectrum Tool)

Xe-135

Xe-133

Xe-133m

I-133

I-132

I-131

Rb-88

Kr-88

Kr-87

Kr-85

Kr-85m

Te-132

Comments

Analysis process basically same as 20_hour_detector2.Chn spectrum. The spectrum was in general well explained.

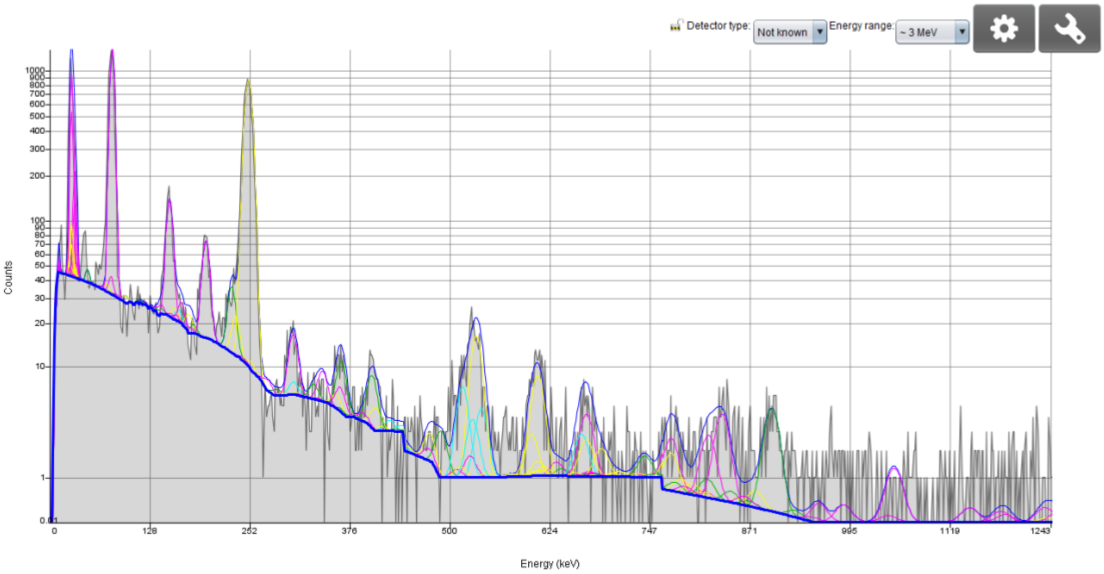

An unexplained peak area remained around 47 keV however.

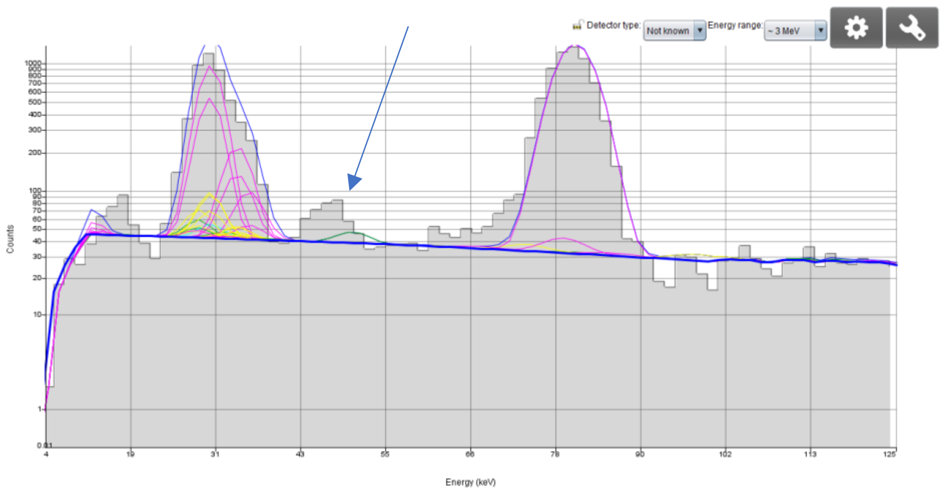

Some analyses of qualitative spectra - Fallout

After the first fallout analysis was made, the rest followed suit immediately. Two examples are given below.

Example 1: 3_day_ground_detector1.Chn

Automatic identification (SpectrumTool):

NuclideIdentification: Bi-214

Category: NORM - Naturally occurring nuclide

ConfidenceClass: 1

Class description:

Small peak

Info:

Characteristic line(s):

609.3 keV (double peak) present with signf.:1.22

Additional lines(s):

1764.5 keV absent with signf.:0.27

1120.3 keV absent with signf.:0.0

NuclideIdentification: Cs-137

Category: IND - Industrial usage nuclide

ConfidenceClass: 1

Class description:

Small peak

Info:

The presence of Am-241, I-131 was excluded

Characteristic line(s):

661.7 keV present with signf.:1.97

NuclideIdentification: Tc-99m

Category: MED - Medical usage nuclide

ConfidenceClass: 3

Class description:

Unequivocal peak

Info:

The presence of Mo-99, U-235, U-238, Tl-201, Se-75, Co-57 was excluded

Characteristic line(s):

140.511 keV present with signf.:5.55

NuclideIdentification: I-123[sh]

Category: MED - Medical usage nuclide

ConfidenceClass: 1

Class description:

Small peak

Info:

The presence of I-123 was excluded

Characteristic line(s):

535.5 keV present with signf.:0.64

NuclideIdentification: I-132M

Category: IND - Industrial usage nuclide

ConfidenceClass: 5

Class description:

Two peaks, at least one clear

Info:

Characteristic line(s):

599.79 keV (yield=14.0%) present with signf.:0.9

772.6 keV (yield=13.9%) present with signf.:1.03

667.71 keV (yield=13.9%) present with signf.:2.3

Additional lines(s):

175.0 keV (yield=8.8%) absent with signf.:0.0

Suggestion: I-131

ConfidenceClass: 0

Class description:

Inconclusive identification

Info:

Characteristic line(s):

364.48 keV (yield=81.5%) present with signf.:4.05

Additional lines(s):

636.98 keV (yield=7.1%) absent with signf.:0.0

284.3 keV (yield=6.1%) absent with signf.:0.34

80.18 keV (yield=2.6%) absent with signf.:0.29

Automatic identification (Unisampo):

```
UniSAMPO 2.72 (1 Apr 2019) Copyrighted 2022-Jan-05 10:47:51
License: Lic. no. 20050608-1, STUK/TKO Helsinki, Finland.
******** R A D I O N U C L I D E   A N A L Y S I S   R E P O R T *********

Un Nuc Nuclide Confid      Activity       Activity       Activity  Error
det lid    name               uBq/m3             Bq      (ccorr) Bq
            set   #

40   1 Ge-75m   1.00           0.000          0.000     151596.328  10.37
2 Kr-85    0.98 2163763314688.000    2163763.250    1548521.750  14.12
98   3 Sr-85    0.98 4006610750889000960.000 4006610731008.000       6877.081  14.12
91   4 Mo-99    0.63           0.000          0.000      57927.473  10.37
89   5 Tc-99m   0.98           0.000          0.000      59246.469  10.37
28   6 Cd-115   0.43           0.000          0.000      64351.012  11.85
15   7 Te-132   0.92           0.000          0.000      30591.941   8.92
 3   8 I-131    0.82           0.000          0.000      75179.266   8.44
99   9 I-132    0.53           0.000          0.000      28855.098   8.12
87  10 I-133    0.86           0.000          0.000      20341.990  11.85
98  11 Cs-134   0.06 57296195584.000      57296.195      10080.427  12.82
15  12 Th-231U  0.39 240531619840.000     240531.625     240531.625  11.90
```

Manual analysis (Spectrum Tool)

Cs-137

Cs-134

Te-132

I-133

I-132

I-132m

I-131

Tc-99m

Mo-99

Comments

The automatic analysis hints at I-131, I-132, Cs-137 and Tc-99m. It is then easy to find Cs-134 and Mo-99. The spectrum is explained reasonably well.

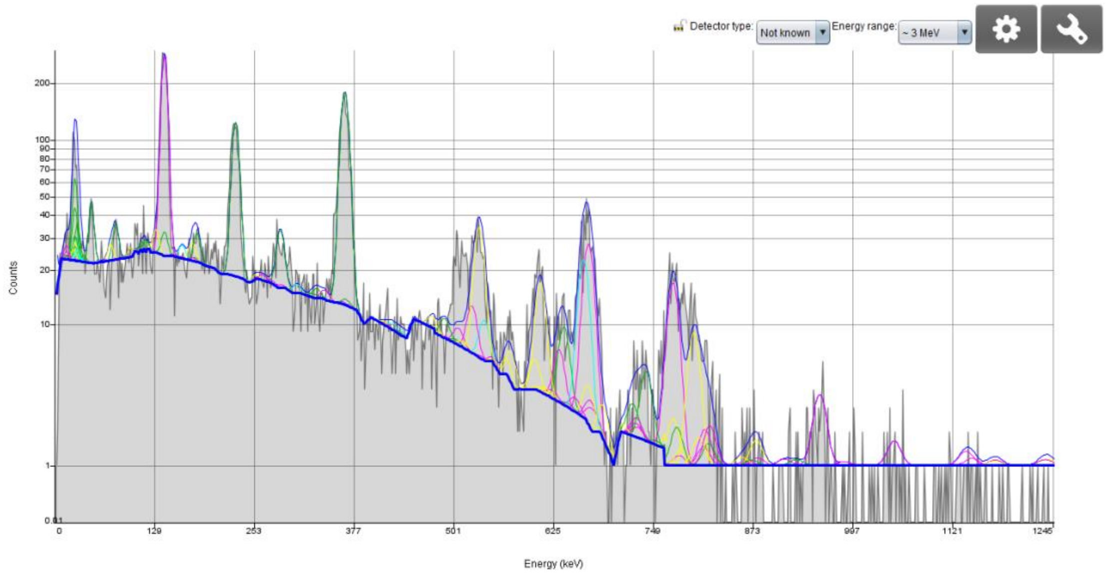

There is an unexplained area left around 510 keV[1].

[1]Post analysis of the simulation input files indicated that two errors were present: the 504 keV peak of I-132 had an erroneously high probability and the I-132 peak at 547 keV had a probability that was too high by a factor of 10.

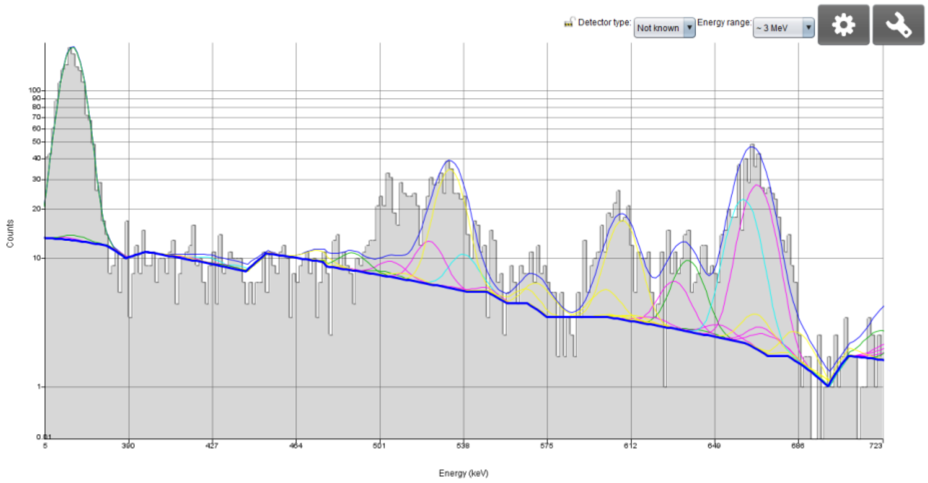

Example 2: 30_day_ground_detector2.Chn

After the first fallout spectrum, this spectrum was easy to analyse.

Automatic identification (SpectrumTool)

Nuclide Identification: Bi-214

Category: NORM - Naturally occurring nuclide

ConfidenceClass: 3

Class description:

Unequivocal peak

Info:

Characteristic line(s):

609.3 keV (double peak) present with signf.:4.5

Additional lines(s):

1764.5 keV absent with signf.:0.0

1120.3 keV absent with signf.:0.0

Nuclide Identification: Cs-137

Category: IND - Industrial usage nuclide

ConfidenceClass: 3

Class description:

Unequivocal peak

Info:

The presence of Am-241, I-131 was excluded

Characteristic line(s):

  661.7 keV present with signf.:3.46

Nuclide Identification: Tc-99m

  Category: MED - Medical usage nuclide

  ConfidenceClass: 2

  Class description:

Small but clear peak

Info:

The presence of Mo-99, U-235, U-238, Tl-201, Se-75, Co-57 was excluded

Characteristic line(s):

  140.511 keV present with signf.:2.44

Nuclide Identification: Cs-134

  Category: SNM - Special nuclear material

  ConfidenceClass: 7

  Class description:

Three or more peaks, two of them unequivocal

Info:

Characteristic line(s):

  604.721 keV present with signf.:4.84

  795.864 keV present with signf.:3.73

Additional lines(s):

  569.331 keV present with signf.:0.67

  127.502 keV absent with signf.:0.0

Suggestion: I-131

ConfidenceClass: 0

Class description:

Inconclusive identification

Info:

Characteristic line(s):

364.48 keV (yield=81.5%) present with signf.:3.41

Additional lines(s):

636.98 keV (yield=7.1%) absent with signf.:0.0

284.3 keV (yield=6.1%) absent with signf.:0.39

80.18 keV (yield=2.6%) absent with signf.:0.39

Automatic identification (Unisampo)

```
UniSAMPO 2.72 (1 Apr 2019) Copyrighted 2022-Jan-05 10:49:51
License: Lic. no. 20050608-1, STUK/TKO Helsinki, Finland.
********  R A D I O N U C L I D E   A N A L Y S I S   R E P O R T  *********

Un Nuc Nuclide Confid      Activity       Activity       Activity  Error
det lid    name               uBq/m3             Bq      (ccorr) Bq
set  #


99   1 Co-58    0.83 1349292.000 1349260279808.000      12731.119 16.63
40   2 Ge-75m   1.00          0.000          0.000      75278.266 10.90
91   3 Mo-99    0.63          0.000          0.000      28765.070 10.90
89   4 Tc-99m   0.98          0.000          0.000      29420.043 10.90
 3   5 I-131    0.72          0.000          0.000      74067.344 10.35
 8   6 Cs-134   0.85 804205712.000     804208.125     141488.656   5.55
85   7 Cs-137   0.93 105672384512.000     105672.383     93802.164 10.58
81   8 Hg-203   0.84 1045556224.000 104555577528.000      6702.010 19.30
```

Manual analysis (Spectrum Tool)

Cs-137

Cs-134

I-131

Tc-99m

Comments

The automatic identifications give a good indication of the possible nuclide content. Analysis was straight forward and the spectrum was well explained.

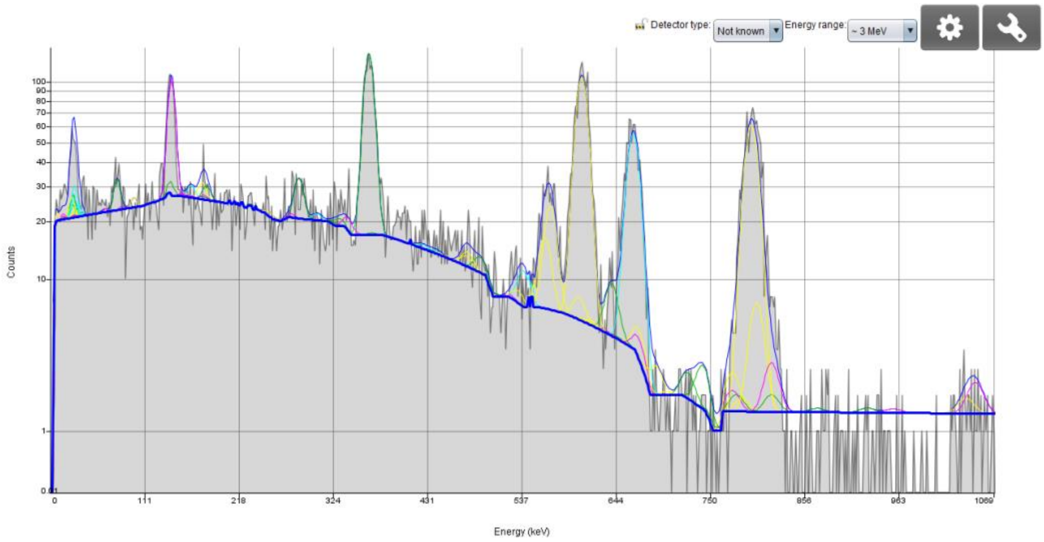

6. Suggestions as to Future Work

$LaBr_3$ detectors exhibit no disadvantages relative to other detector types with respect to deployment for direct measurement of fallout nuclides in the situations as outlined in this report. They are comparable to NaI and HPGe with respect to efficiency and outperform NaI in relation to resolution. No indication was provided in the project as to difficulties with respect to the application of conventional software routines to the analysis of accrued. A difficulty is apparent with respect to efficiency calibration of $LaBr_3$ detectors for direct measurement of airborne activity and, to a lesser extent, ground deposited activity although this difficulty is similar to that encountered for all detector types.

Calibration of detectors for direct measurement of airborne activity will almost always be by mathematical methods. In this regard, use may either be made of analytical functions or some kind of Monte Carlo approach. The former has the advantage of speed and relative simplicity, the latter has the advantage in providing (arguably) a better representation of the physical reality of the situation. Both are hampered by, in this case, a relative lack of information as the construction of the detector and its housing. The latter is a severe disadvantage due to the necessity to bring computing assets to bear that are not available to the average user. Either method can generate values that are, to a large extent, comparable with each other but which include significant uncertainties due to the reasons outlined previously.

Elimination of a large proportion of these uncertainties could possibly be achieved by a detailed study of the detectors – this would entail the generation of accurate and precise information as to the structures surrounding the detectors as well as the crystal themselves. Once achieved, a series of precisely controlled laboratory experiment would be required to validate the MC model of the detector.

The validated model could then be used to optimize the geometry to be employed for assessment of efficiency with respect to generation of data of acceptable accuracy and precision for the purposes to which the detector will be employed within simulation time frames that are practicable.

8. References

Agostinelli, S., Allison, J., Amako, K., Apostolakis, J., Araujo, H., Arce, P., Asai, M., Axen, D., Banerjee, S., Barrand, G., Behner, F., Bellagamba, L., Boudreau, J., Broglia, L., Brunengo, A., Burkhardt, H., Chauvie, S., Chuma, J., Chytracek, R., Cooperman, G., Cosmo, G., Degtyarenko, P., Dell'Acqua, A., et al., 2003, Geant4—a simulation toolkit, Nucl. Instrum. Methods. Phys. Res. B https://doi.org/10.1016/S0168-9002(03)01368-8.

Jednorog, S., Ciupek, K., Krajewski, P., Laszynska, E. Ziolkowski, A., 2015. Calibration of the Angular Energy Efficiency of an In-situ Spectrometer Based on a LaBr3(Ce) Detector, Journal of Radioanalytical and Nuclear Chemistry, 305, pp. 567-571

Johansson, J., Kock, P., Boson, J., Karlsson, S., Isaksson, P., Lindgren, J., Tengborn, E., Blixt Buhr, A.M., Bäverstam, U. 2019. Review of Swedish emergency planning zones and distances, Appendix 3, Report number: 2017:27e ISSN: 2000-0456. 91 p.

Modzelewski, L., Jednorog, S., Woloszczuk, K., Krajewski, P., Mazur, L., Klis, B., Baranowska, Z., Jakubowska, A., Norenberg, M., Kawalec, A., Skrzynski, W. 2021. Dependence of Photon Registration Efficiency on LaBr3(Ce) Detector Orientation for In-situ Radionuclide Monitoring, Applied Radiation and Isotopes: 178 pp. 109974

Toivonen, H., Mattila, A., Vesterbacka, K. Efficiency Calibration for in-situ Gamma Spectrometry of Airborne Acitivity and Fallout. TTL-TECDOC-2009-018.

Urban, T. and Vágner, P., 2019, Simulation of the Response of a $LaBr_3(Ce)$ Detector in an Atmosphere Contaminated with Radionuclides After a Nuclear Power Plant Accident, Radiation Protection Dosimetry, 186: 2–3, pp. 346–350

Bibliographic Data Sheet **NKS-453**

Title	Analysis of the Performance of $LaBr_3$ Detectors for Fresh Fallout Response (PERLAD)
Author(s)	M.Dowdall[1], Kari Peräjärvi[2], Tero Karhunen[2], Sara Ehrs[3], Charlotte Alfast Espensen[4], Gísli Jónsson[5]
Affiliation(s)	[1]Norwegian Radiation and Nuclear Safety Authority [2] Radiation and Nuclear Safety Authority (STUK), Finland [3] Swedish Radiation Safety Authority [4] Danish Emergency Management Agency (DEMA) [5] Icelandic Radiation Safety Authority
ISBN	978-87-7893-546-5
Date	January 2022
Project	NKS-B / PERLAD
No. of pages	56
No. of tables	16
No. of illustrations	21
No. of references	5
Abstract max. 2000 characters	With spectral resolution of approximately 3 % at 662 keV, $LaBr_3$ scintillators exhibit substantial improvements over sodium iodide scintillators with a resolution of 6-7 % for crystals of comparable sizes and fast emission relative to NaI and HPGe. $LaBr_3$ crystals are available in sizes up to 3×3 inches and this availability has led to an increase in the prevalence of such detectors for a variety of purposes. These include as hand held detectors for in-field use, in conventional laboratory situations and for direct monitoring of radioactive contaminants. Direct measurement of airborne contamination is made complicated for any detector type due to the necessity to generate efficiency data for a geometry which is in effect impossible to replicate. While estimates of efficiency may be obtained using deterministic calculations, the need to account for elements of the detector assembly aside from the detector complicates the process. This project investigates the use of such detectors for the direct measurement of airborne and ground deposited contamination using Monte Carlo simulation for the assessment of efficiency in field use configurations.
Key words	$LaBr_3$, efficiency, Monte Carlo, emergency preparedness

Available on request from the NKS Secretariat, P.O.Box 49, DK-4000 Roskilde, Denmark.
Phone (+45) 4677 4041, e-mail nks@nks.org, www.nks.org